Neogene to Quaternary broken foreland formation and sedimentation dynamics in the Andes of NW Argentina (25°S)

M. P. Hain,[1,2] M. R. Strecker,[1] B. Bookhagen,[3] R. N. Alonso,[4] H. Pingel,[1] and A. K. Schmitt[5]

Received 14 March 2010; revised 27 November 2010; accepted 20 December 2010; published 16 March 2011.

[1] The northwest Argentine Andes constitute a premier natural laboratory to assess the complex interactions between isolated uplifts, orographic precipitation gradients, and related erosion and sedimentation patterns. Here we present new stratigraphic observations and age information from intermontane basin sediments to elucidate the Neogene to Quaternary shortening history and associated sediment dynamics of the broken Salta foreland. This part of the Andean orogen, which comprises an array of basement-cored range uplifts, is located at ~25°S and lies to the east of the arid intraorogenic Altiplano/Puna plateau. In the Salta foreland, spatially and temporally disparate range uplift along steeply dipping inherited faults has resulted in foreland compartmentalization with steep basin-to-basin precipitation gradients. Sediment architecture and facies associations record a three-phase (~10, ~5, and <2 Ma), east directed, yet unsystematic evolution of shortening, foreland fragmentation, and ensuing changes in precipitation and sediment transport. The provenance signatures of these deposits reflect the trapping of sediments in the intermontane basins of the Andean hinterland, as well as the evolution of a severed fluvial network. Present-day moisture supply to the hinterland is determined by range relief and basin elevation. The conspiring effects of range uplift and low rainfall help the entrapment and long-term storage of sediments, ultimately raising basin elevation in the hinterland, which may amplify aridification in the orogen interior. **Citation:** Hain, M. P., M. R. Strecker, B. Bookhagen, R. N. Alonso, H. Pingel, and A. K. Schmitt (2011), Neogene to Quaternary broken foreland formation and sedimentation dynamics in the Andes of NW Argentina (25°S), *Tectonics*, *30*, TC2006, doi:10.1029/2010TC002703.

1. Introduction

[2] Broken forelands are an integral part of many orogens. For example, today such systems characterize parts of the Colombian Andes [e.g., *Mora et al.*, 2006, 2009; *Parra et al.*, 2009a, 2009b], the Tian Shan [e.g., *Sobel and Dumitru*, 1997; *Sobel et al.*, 2003], the Qilian Shan [e.g., *Tapponnier et al.*, 1990], and the Salta foreland of northwest Argentina (Figure 1) [e.g., *Allmendinger et al.*, 1983] (also this study). The geologic record holds more examples, including the Cretaceous-Eocene Laramide province of North America [e.g., *Jordan and Allmendinger*, 1986; *Talling et al.*, 1995; *Marshak et al.*, 2000; *Davis et al.*, 2009; *Ernst*, 2010] and the Paleozoic Alice Springs broken foreland in Australia [*Haines et al.*, 2001]. In these environments, patterns of deformation, sediment routing and accumulation are different from thin-skinned foreland fold-and-thrust belts [e.g., *DeCelles and Giles*, 1996] and may be characterized by highly disparate spatiotemporal patterns of deformation and sedimentation (Figure 1) [e.g., *Strecker et al.*, 2011].

[3] Over recent years a conceptual framework for the interactions between tectonic forcing, climatic conditions and sediment dynamics in broken forelands has been proposed [*Sobel et al.*, 2003; *Sobel and Strecker*, 2003; *Hilley and Strecker*, 2005; *Strecker et al.*, 2007a, 2009, 2011]. In summary, these models posit that reactivation of basement anisotropies and spatiotemporally disparate patterns of range uplifts lead to the formation of highly localized depocenters that may experience aridification when the frontal ranges attain laterally continuous threshold topography, which is able to block moisture-bearing winds. Ensuing basin-scale sediment storage within the intermontane basins is driven by tectonic fragmentation of the drainage system and may be enhanced by orographic shielding, which reduces precipitation, discharge, river transport capacity, and ultimately river incision rates in the hinterland. Accordingly, sediment provenance in the deposits of the foreland should change drastically when range uplift severs drainage conditions and traps sediment in the hinterland. In this study we evaluate this prediction by providing an account of the facies, provenance signatures, and distribution of syntectonic deposits of the broken Salta foreland of northwestern Argentina at approximately 25°S (Figure 1).

[4] Despite great interest in the interaction between tectonics, climate and sediment dynamics, the age of uplift of

[1]DFG-Leibniz Center for Earth Surface Process and Climate Studies, Institut für Geowissenschaften, Universität Potsdam, Potsdam, Germany.
[2]Department of Geosciences, Princeton University, Princeton, New Jersey, USA.
[3]Geography Department, University of California, Santa Barbara, California, USA.
[4]Facultad de Ciencias Naturales, Universidad Nacional de Salta, Salta, Argentina.
[5]Department of Earth and Space Sciences, University of California, Los Angeles, California, USA.

0278-7407/11/2010TC002703

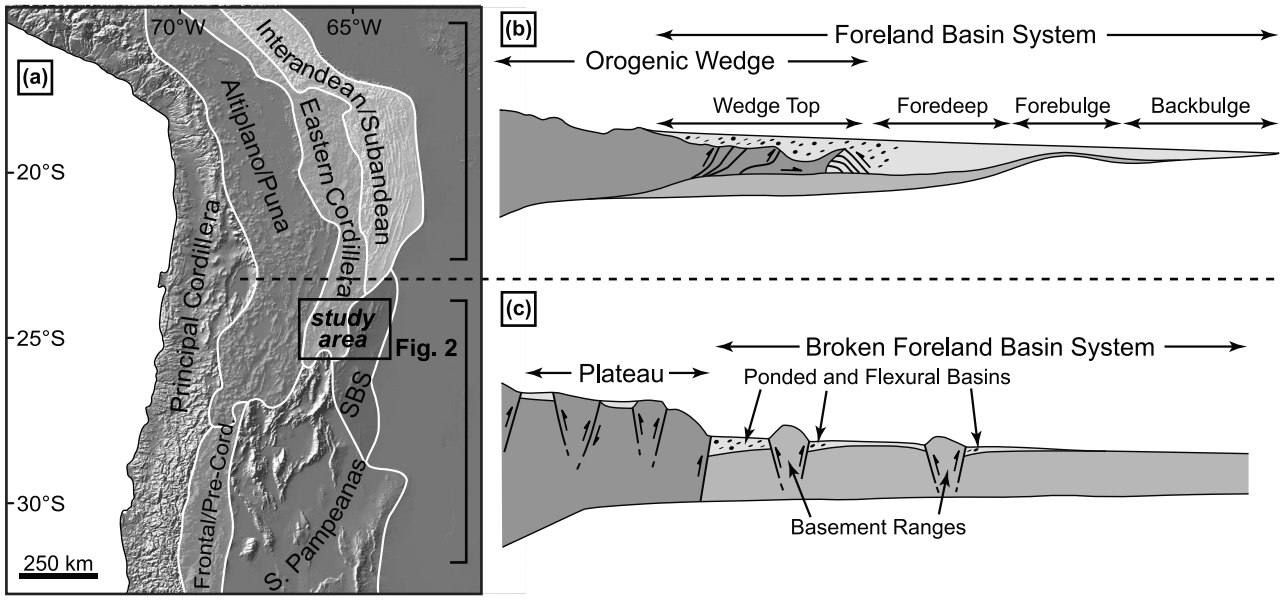

Figure 1. (a) Overview of the morphotectonic domains of the central Andes and schematic representation of (b) the thin-skinned Subandean foreland fold-and-thrust belt and (c) the thick-skinned broken foreland system farther to the south (modified after *Strecker et al.* [2011] (with kind permission of Blackwell) and *DeCelles and Giles* [1996] (with kind permission of John Wiley)). The box in Figure 1a marks the study area (Figure 2). The dashed line at 23.5°S represents the transition in tectonic style of the retroarc foreland of the southern central Andes.

many ranges that presently compartmentalize the Salta foreland is unknown, especially in the eastern sector [cf. *Reynolds et al.*, 2000]. The deformation history is only adequately resolved in the arid, well exposed western sector of the foreland, along the eastern flanks of the Puna Plateau [*Salfity et al.*, 2004; *Deeken et al.*, 2006; *Coutand et al.*, 2006; *Hongn et al.*, 2007; *Mortimer et al.*, 2007; *Carrapa et al.*, 2008; *Carrera and Muñoz*, 2008; *Bosio et al.*, 2009; *Bywater-Reyes et al.*, 2010].

[5] Our study specifically examines the heavily vegetated eastern sector of the Salta foreland whereby we are trying to resolve the following questions: When was the foreland compartmentalized by range uplifts? How did deformation modify sediment dynamics? Was sediment transiently trapped in the intermontane basins or exported from the orogen? To answer these questions we first present a detailed introduction to the basement lithologies and the stratigraphic record of the region, which forms the foundation for the synthesis we are attempting to accomplish. Second, we present an account of tectonostratigraphic relationships of late Mio-Pliocene and Quaternary strata. Third, changes of the conglomerate provenance signatures and facies pertaining to three syntectonic formations allow to distinguish between sediment export from the orogen versus sediment trapping in the hinterland. Fourth, we undertake a detailed analysis of present-day geomorphic and climatological conditions. Overall, our observations agree well with and add detail to the model outlined above. Importantly, we will use observations to illustrate (1) that efficient intermontane sediment trapping does not require internal drainage conditions and (2) that intermontane sediment storage may modify precipitation patterns by raising basin elevation in the hinterland.

2. Geologic Setting

[6] The study area is situated at ~25°S, between the arid, internally drained orogenic Puna Plateau in the west and the undeformed Chaco Plain foreland basin in the east. Specifically, this region comprises the southern sectors of the Eastern Cordillera (EC), the Santa Barbara System (SBS), and the Sierras Pampeanas morphotectonic provinces (Figures 1 and 2b); here, we refer to the study area as a whole as the "Salta foreland." At this latitude the Andean orogen was, until the middle Miocene, bordered by a contiguous foreland basin [e.g., *Coutand et al.*, 2001; *Hernández et al.*, 2005; *Carrapa et al.*, 2008; *Bosio et al.*, 2009]. Since that time, contractile inversion of the Cretaceous Salta Rift [e.g., *Baldis et al.*, 1976; *Rolleri*, 1976; *Bianucci and Homovec*, 1982; *Salfity*, 1982; *Allmendinger et al.*, 1983; *Marquillas and Salfity*, 1988; *Mon and Salfity*, 1995; *Grier et al.*, 1991; *Viramonte et al.*, 1999; *Kley and Monaldi*, 2002; *Kley et al.*, 2005; *Carrera et al.*, 2006; *Carrera and Muñoz*, 2008] has led to a patchwork of basement-cored ranges and intervening intermontane basins that have experienced episodes of internal, or reduced external, drainage conditions [e.g., *Malamud et al.*, 1996; *Bookhagen et al.*, 2001; *Salfity et al.*, 2004], but have been recaptured by rivers that are adjusted to the undeformed foreland (Figure 2a).

[7] Inversion of Cretaceous normal faults constitutes the primary mode of Neogene contractile reactivation in both the SBS [e.g., *Mon and Salfity*, 1995; *Kley and Monaldi*,

2002] and the EC [e.g., *Carrera et al.*, 2006]. The Cretaceous Salta Rift was characterized by a series of subbasins distributed around the Salta-Jujuy High, a central horst area of the former rift system [*Marquillas and Salfity*, 1988]. The inverted rift subbasins within the Salta foreland are structurally linked by an inferred detachment horizon at a depth of 10 to 16 km that dips gently toward the west [*Grier et al.*, 1991; *Kley and Monaldi*, 2002; *Carrera et al.*, 2006]. The normal faults of the former rift generally strike NNE-SSW and many of them dip to the east, toward the present-day foreland [e.g., *Grier et al.*, 1991]. However, in the vicinity of the city of Salta (i.e., the Salta-Jujuy High; see section 2.2 and Figure 2a), reactivated Neogene contractional structures strike strictly N–S and are thought to have been guided by Paleozoic thrusts faults, extensional fault arrays, and metamorphic foliations [e.g., *Mon and Hongn*, 1991; *Hongn and Riller*, 2007; *Wegmann et al.*, 2008; *Hongn et al.*, 2008]. In fact, *Hongn et al.* [2010] recently documented that these older basement fabrics have also influenced the Cretaceous Salta Rift. Although these principle structures are well described the timing when they compartmentalized the foreland sector remains largely unresolved.

[8] In sections 2.1–2.4 we provide a detailed synopsis of the rich lithologic and stratigraphic database of the region. This information serves as a backdrop to understanding the tectonic significance of the provenance signatures that we document.

2.1. Basement Rocks

[9] A suite of different metamorphic grades and distinct N–S oriented tectonometamorphic domains characterize the basement beneath the Salta foreland [*Mon and Hongn*, 1991; *Mon and Salfity*, 1995]. Most relevant to this study is an Ordovician-Silurian orogenic belt that exposes a basement composed mainly of gneisses, mylonites and Precambrian granitoid batholiths [*Mon and Hongn*, 1991; *Salfity et al.*, 1998]. This tectonometamorphic domain along the former western margin of Gondwana broadly coincides with the present-day boundary between the Puna Plateau and the EC [e.g., *Allmendinger et al.*, 1983; *Mon and Hongn*, 1991; *Hongn and Riller*, 2007]. It has been suggested that the lithologic transition at the Puna/EC boundary is ultimately related to a Mesoproterozoic suture formed during the assembly of Rodinia [see *Ramos*, 2008, and references therein]. Consequently, Neogene reverse faults at the Puna Plateau margin (westernmost EC) expose only amphibolites and migmatites together with plutonic and pegmatitic rocks (high-grade basement in Figure 2a), whereas greenschist-facies metasedimentary rocks of the Puncoviscana Formation (low-grade basement in Figure 2a) are exposed throughout the central and eastern EC and the SBS [e.g., *Ruíz Huidobro*, 1968; *Ježek et al.*, 1985; *Mon and Hongn*, 1991; *Salfity et al.*, 1998; *Ramos*, 2008]. However, in the vicinity of Metán (i.e., Sierra de Metán), recrystallization, still under greenschist metamorphic conditions, resulted in a regionally distinct lithology that has been grouped into the Medina Formation [e.g., *Salfity et al.*, 1998] (Figure 2a). In contrast to the Puncoviscana Formation, this unit contains macroscopic mica and chlorite and displays folds with wavelengths of up 20 cm [*Durand and Rossi*, 1999]. The Cumbres del Castillejo expose black carbonates of the Las Tienditas Formation dating back to the Precambrian/Phanerozoic boundary [*Sial et al.*, 2001]. The basement rocks of the Sierra de Ovejeria and the Metán ranges expose light gray, hornblende-bearing volcanic rocks associated with Cretaceous rift-related magmatism [*Viramonte et al.*, 1999]. With respect to the objectives of this study, the latter three units (i.e., Medina Formation, Las Tienditas Formation and light gray volcanics) are important for sediment provenance determination because they provide excellent marker lithologies with well-defined source regions.

2.2. Paleozoic, Mesozoic, and Paleogene Sedimentary Successions

[10] Paleozoic strata of the Salta foreland include shales, lithic sandstones, and pebbly quartz arenites [e.g., *Ruíz Huidobro*, 1968; *Turner*, 1970], limited to areas northeast of the NW-SE striking El Toro lineament [*Allmendinger et al.*, 1983] (Paleozoic strata in Figure 2a). During the extension that generated the Cretaceous Salta Rift this lineament constituted the southwestern limit of the Salta-Jujuy High. Consequently, the clastic and volcanic Cretaceous rift fill (Pirgua Subgroup) as well as carbonates and shales (Balbuena and Santa Bárbara subgroups; Paleogene strata in Figure 2a) deposited in the basins during postrifting thermal subsidence, occur only southwest of the lineament [e.g., *Grier et al.*, 1991; *Salfity et al.*, 1998]. Although the lithologic contrast across the El Toro lineament suggests a fault that was active during both the Paleozoic and the Cretaceous, in the absence of unambiguous observations concerning its Cenozoic tectonic activity, we simply note its importance as a discriminator for sediment provenance.

[11] The upper section of the Santa Bárbara Subgroup and coeval units farther west exhibit early signs of contractional

Figure 2. Overview of the Salta foreland. (a) Geologic map simplified after the Salta province map issued by the Argentinean Geologic Survey SEGEMAR [i.e., *Salfity et al.*, 1998] and (b) SRTM topography (U.S. Geological Survey) of the study area. See Figure 1a for location. The names of selected ranges and basins are shown in white, and towns are shown in black font. Paleoflow directions derived from clast imbrications are shown in Figure 2b; the labels correspond to the stations of Figure 6. The paleoflow directions from the Calchaquí Valley [*Richter*, 2002, also unpublished data, 2002] pertain to the San Felipe Formation, which is coeval with the Piquete Formation (see Figure 3); the two paleoflow directions at the northern edge have been measured on conglomerates in the Quebrada del Toro Basin [*Hilley and Strecker*, 2005], which are coeval with the Guanaco and Piquete formations. For details on the lithologic units shown in Figure 2a see sections 2.1 and 2.2. Yellow stars in Figure 2b mark the sample sites for volcanic ashes pertaining to the La Troja Formation (see section 3.1). Magmatic centers exposing hornblende-bearing subvolcanic rocks are present in the Ovejeria and Metán ranges, but their spatial extent is below the scale of the geologic map.

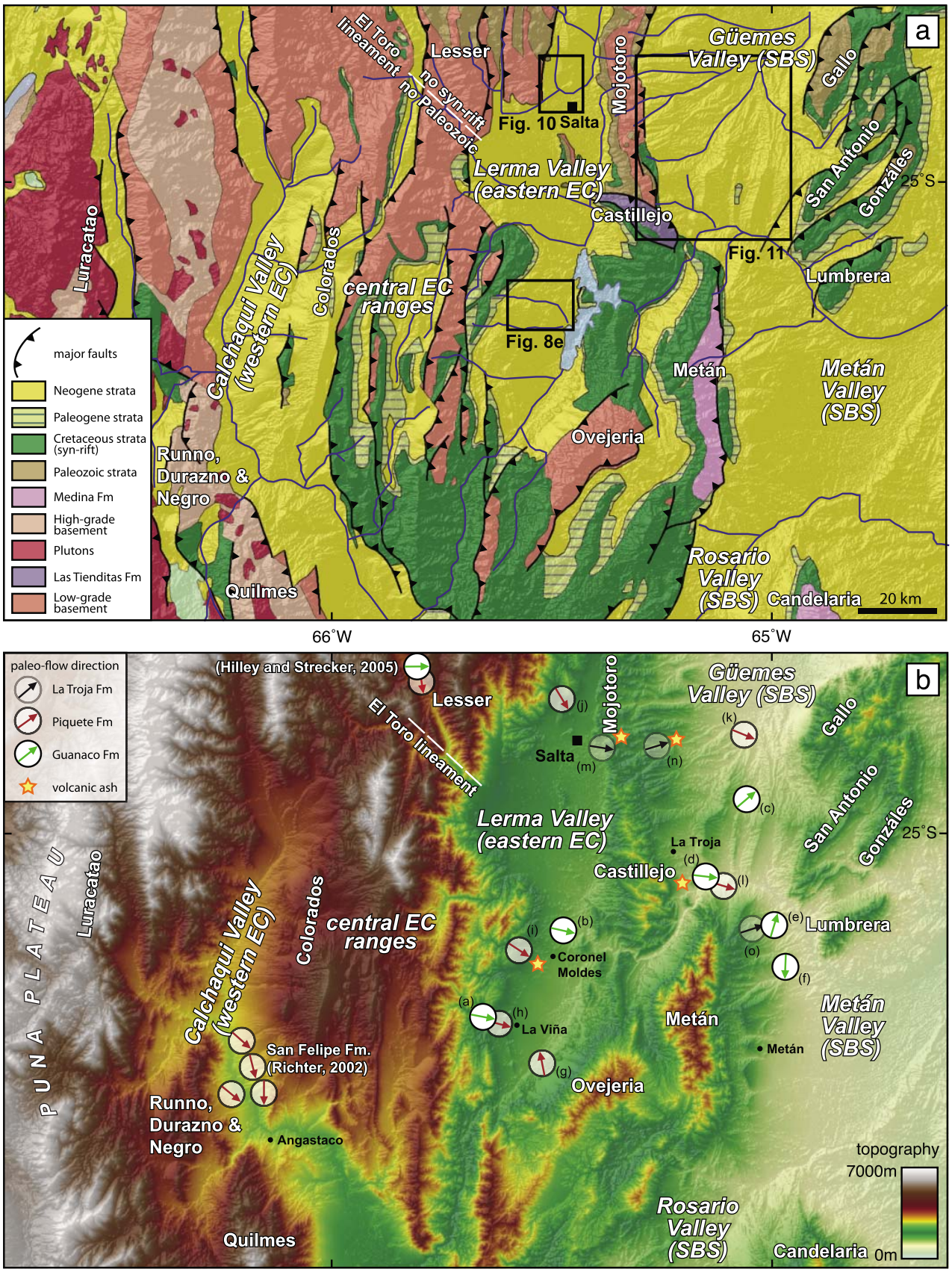
a
El Toro lineament
Lesser
no syn-rift
no Paleozoic
Fig. 10 Salta
Mojotoro
Güemes Valley (SBS)
Gallo
San Antonio
Gonzáles
25°S
Lerma Valley (eastern EC)
Castillejo
Fig. 11
Lumbrera
Luracatao
Calchaqui Valley (western EC)
Colorados
central EC ranges
Fig. 8e
Metán
Metán Valley (SBS)
Ovejeria
Runno, Durazno & Negro
Rosario Valley (SBS)
Candelaria
20 km
Quilmes
major faults
Neogene strata
Paleogene strata
Cretaceous strata (syn-rift)
Paleozoic strata
Medina Fm
High-grade basement
Plutons
Las Tienditas Fm
Low-grade basement
66°W
65°W
b
paleo-flow direction
La Troja Fm
Piquete Fm
Guanaco Fm
volcanic ash
(Hilley and Strecker, 2005)
Lesser
El Toro lineament
Mojotoro
Güemes Valley (SBS)
Gallo
Salta
San Antonio
Gonzáles
25°S
Lerma Valley (eastern EC)
La Troja
Castillejo
PUNA PLATEAU
Luracatao
Calchaqui Valley (western EC)
Colorados
central EC ranges
Lumbrera
Coronel Moldes
La Viña
San Felipe Fm. (Richter, 2002)
Metán
Metán Valley (SBS)
Ovejeria
Runno, Durazno & Negro
Angastaco
topography
7000m
0m
Rosario Valley (SBS)
Candelaria
Quilmes

Figure 2

deformation. For example, growth strata preserved along the present-day Puna margin provide clear evidence for Eocene to Oligocene tectonism giving rise to foreland-basin style sedimentation [e.g., *Hongn et al.*, 2007; *Bosio et al.*, 2009]. Proximal and distal units pertaining to this early stage of Andean evolution are well documented [e.g., *Vergani and Starck*, 1989a, 1989b; *Salfity et al.*, 1993; *Starck and Vergani*, 1996].

2.3. Metán Subgroup

[12] Following the establishment of internal drainage in the Puna region during the middle Miocene [e.g., *Jordan and Alonso*, 1987; *Alonso et al.*, 1991; *Vandervoort et al.*, 1995] foreland-style sedimentation continued unconformably atop Paleogene strata [e.g., *Hongn et al.*, 2007]. In the eastern EC and the SBS, the Neogene Metán Subgroup (Orán Group) is composed of sandstones and mudstones, with occasional beds of oolitic limestones [e.g., *Russo and Serraiotto*, 1978; *Galli et al.*, 1996]. These horizons pertaining to the Anta Formation have been associated with the Paranense transgression between 15 and 13 Ma [e.g., *Hernández et al.*, 2005]. The transition from the thinly bedded Anta Formation to the overlying sandstone-dominated Jesus Maria Formation (eastern EC and the SBS) defines an upward coarsening and thickening trend. Distinct lateral facies zonation recorded in the EC [*Russo and Serraiotto*, 1978] furthermore enables a correlation with the coeval conglomerates and sandstones of the Angastaco Formation of the western EC (Calchaquí Valley) (Figure 3), related to deposition in a braidplain environment [*Díaz and Malizzia*, 1984].

2.4. Jujuy Subgroup

[13] The Jujuy Subgroup (Orán Group) is currently subdivided into the Guanaco and Piquete formations [*Gebhard et al.*, 1974; *Russo and Serraiotto*, 1978; *Starck and Vergani*, 1996]. In addition to these late Miocene to early Pleistocene formations we document evidence for thick Quaternary strata exposed in both the EC and the SBS, constituting a new unit, the La Troja Formation.

2.4.1. Guanaco Formation

[14] The well-sorted sandstones, gravelly sandstones, and intraformational conglomerates of the Guanaco Formation overlie the Metán Subgroup. The appearance of conglomerates and the meter- to decameter-scale bedding is the continuation of the upward coarsening and thickening trend that commenced in the Metán Subgroup. Within the SBS, the Guanaco Formation is characterized by multiple sharp transitions from mudstones to conglomerates and sandstones. Mudstones are less abundant in the EC, where well-sorted sandstones dominate the formation, together with conglomeratic and gravelly sandstone channels that form sharp contacts with the well-sorted sandstones. Matrix-supported conglomerates are common in both the EC and the SBS [*Gonzalez Villa*, 2002], mostly associated with small-scale cut-and-fill geometries and planar cross stratification. The basal contact with the Metán Subgroup has been reported as being conformable to erosive [e.g., *Gebhard et al.*, 1974], but *Cristallini et al.* [1997] recognized an onlap relationship in the SBS, possibly related to an early uplift at the EC/SBS transition [*Hain*, 2008] (also this study). In the seismic reflection data presented below it will be shown that a low-amplitude angular unconformity also exists in the eastern EC.

[15] The Guanaco Formation was deposited between >10.9 and <6.9 Ma [*Viramonte et al.*, 1994; *Reynolds et al.*, 2000]. In the vicinity of Coronel Moldes (Figure 2) we dated a volcanic ash layer at 9.31 ± 0.31 Ma (Figure 4a and Table 1; see also section 3.1) from within a Guanaco Formation sandstone sequence with scarce granitoid clast bearing conglomeratic channels. Farther west, along the Puna margin, the Palo Pintado Formation (Calchaquí Valley western EC) was deposited between 9 ± 1 Ma and <5.27 ± 0.28 Ma [*Coutand et al.*, 2006] in an unrestricted foreland setting with longitudinal rivers, swamps and ponds [*Starck and Anzótegui*, 2001]. This is interesting because, we will argue below, the Palo Pintado and Guanaco formations comprise a megafan system that delivered sediment with a Puna border provenance signature across the entire foreland sector.

2.4.2. Piquete Formation

[16] The Piquete Formation erosionally to paraconformably overlies the Guanaco Formation in the SBS [*Cristallini et al.*, 1997] and the eastern part of the EC, whereas these formations are separated by an angular unconformity in the central EC [*Gonzalez Villa*, 2002; *Carrera and Muñoz*, 2008]. In the eastern sector of the EC, the Piquete Formation comprises well imbricated, clast-supported, and laterally continuous conglomerate horizons interbedded with silty sandstones. In the SBS, the Piquete Formation is characterized by abundant carbonate-bearing paleosols interbedded with gravelly sandstones and conglomerates that are predominantly matrix supported. The channel facies frequency and the modal clast size of the associated conglomerates tend to decrease from the EC to the SBS.

[17] Based on magnetostratigraphic data and an apatite fission track dated tuff near Coronel Moldes in the Lerma Valley, the Piquete Formation was deposited between ~5 [*Reynolds et al.*, 1994, 2000] and <1.3 ± 0.2 Ma [*Malamud et al.*, 1996]. These strata are thus coeval with the San Felipe Formation in the Calchaquí Valley to the west [*Coutand et al.*, 2006; *Strecker et al.*, 2007a] (Figure 3).

2.4.3. La Troja Formation

[18] Only two reports have addressed the accumulation of thick Quaternary strata in the eastern EC and the SBS [*Monaldi et al.*, 1996; *Carrera and Muñoz*, 2008]. *Monaldi et al.* [1996] attribute these deposits to the Piquete Formation. Noting both growth strata and unroofing trends in conglomerate composition they propose two Pleistocene thrust fronts, one in the central EC and one at the EC/SBS transition, as the sediment source regions. *Carrera and Muñoz* [2008] briefly mention Quaternary growth strata in the eastern EC, complimentary to a wealth of similar Quaternary structures they document in the western and central EC. Furthermore, *Salfity et al.* [2004] documented lake deposits ponded west of a Quaternary fault in the western EC. Below we present previously unpublished observations pertaining to the

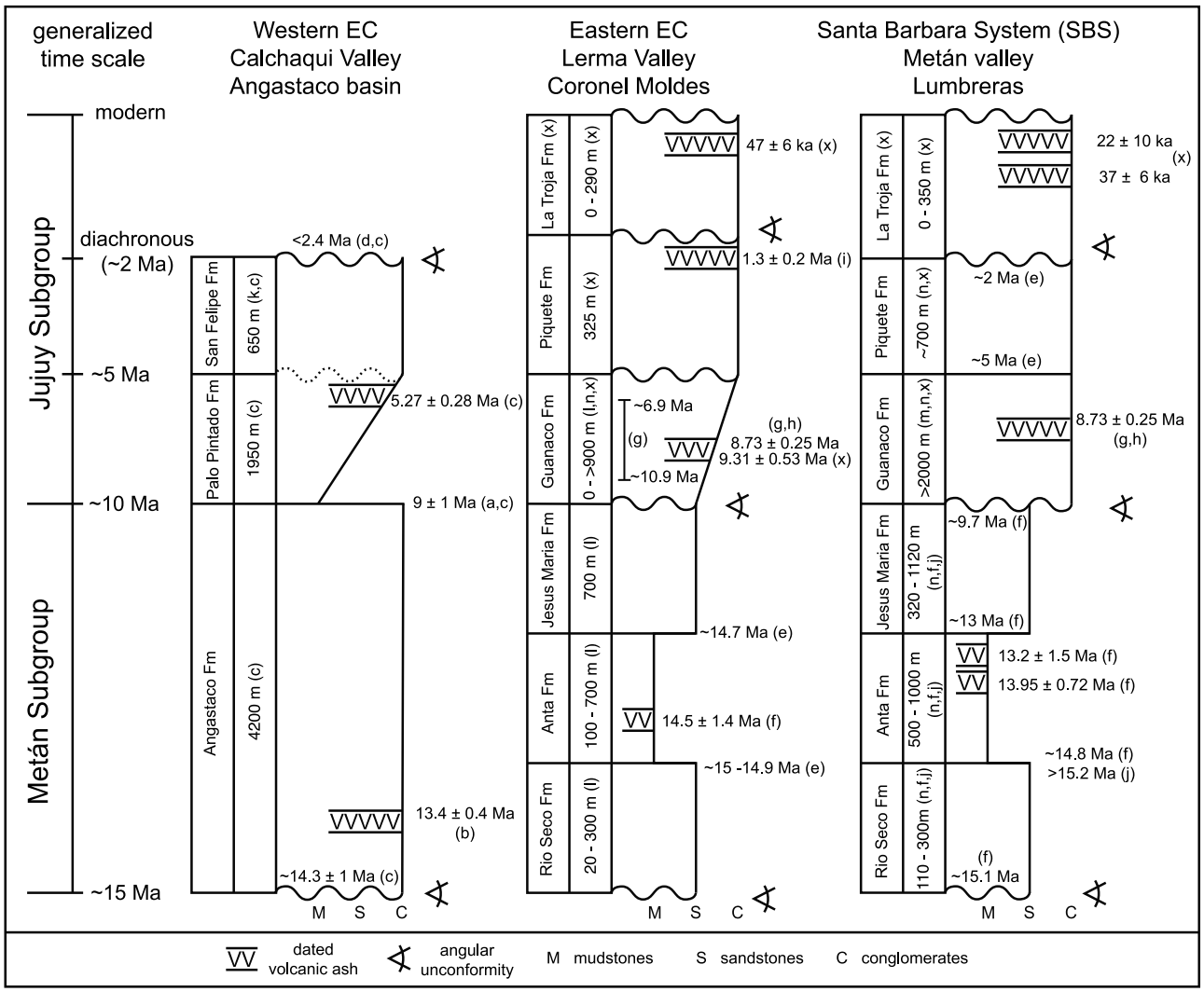

Figure 3. Compilation of Neogene stratigraphy and chronologic constraints for the three principle intermontane basins east of the Puna margin. The thicknesses of the formations are not shown to scale as they have been aligned to a generic time scale that also corresponds to megasequences II to IV of *Starck and Vergani* [1996]. Note that, especially at the Piquete/La Troja contact, diachronous onset of deformation/syntectonic deposition is implicated. Deposits in the Calchaquí Valley equivalent to the La Troja Formation have not been investigated herein, but *Carrera and Muñoz* [2008] and *Salfity et al.* [2004] reported Quaternary strata closely associated with neotectonic compressional structures. Compilation based on the following: a, *Marshall et al.* [1983]; b, *Grier and Dallmeyer* [1990]; c, *Coutand et al.* [2006]; d, M. R. Strecker (unpublished data, 2001); e, *Reynolds et al.* [1994]; f, *Reynolds et al.* [2000]; g, *Viramonte et al.* [1994]; h, *Viramonte et al.* [1984]; i, *Malamud et al.* [1996]; j, *Galli et al.* [1996]; k, *Grier* [1990]; l, *Vergani and Starck* [1988]; m, *Gebhard et al.* [1974]; n, *Gonzalez Villa* [2002]; x, this study.

Quaternary deposits [*Hain*, 2008] and suggest the adoption of the name "La Troja Formation."

3. Methods

3.1. U-Pb and U-Th Zircon Geochronology

[19] It is important for our assessment of the stratigraphic record of the poorly exposed, heavily vegetated eastern sector of the Salta foreland that we assign our observations to the correct formations. For this reason we radiometrically dated zircons from five volcanic ash samples, one pertaining to the inferred megafan deposit (Guanaco Formation) and four pertaining to the sediments deposited during and after the latest stage of intrabasin deformation (La Troja Formation; sample sites marked as yellow stars in Figure 2b). U-Pb and U-Th zircon ages were obtained using the CAMECA IMS 1270 ion microprobe at UCLA (Tables 1 and 2). Instrument setup and relative sensitivity calibrations for U-Pb and U-Th analysis are described by *Grove et al.* [2003] and *Schmitt et al.* [2006]. U-Pb age uncertainties estimated from

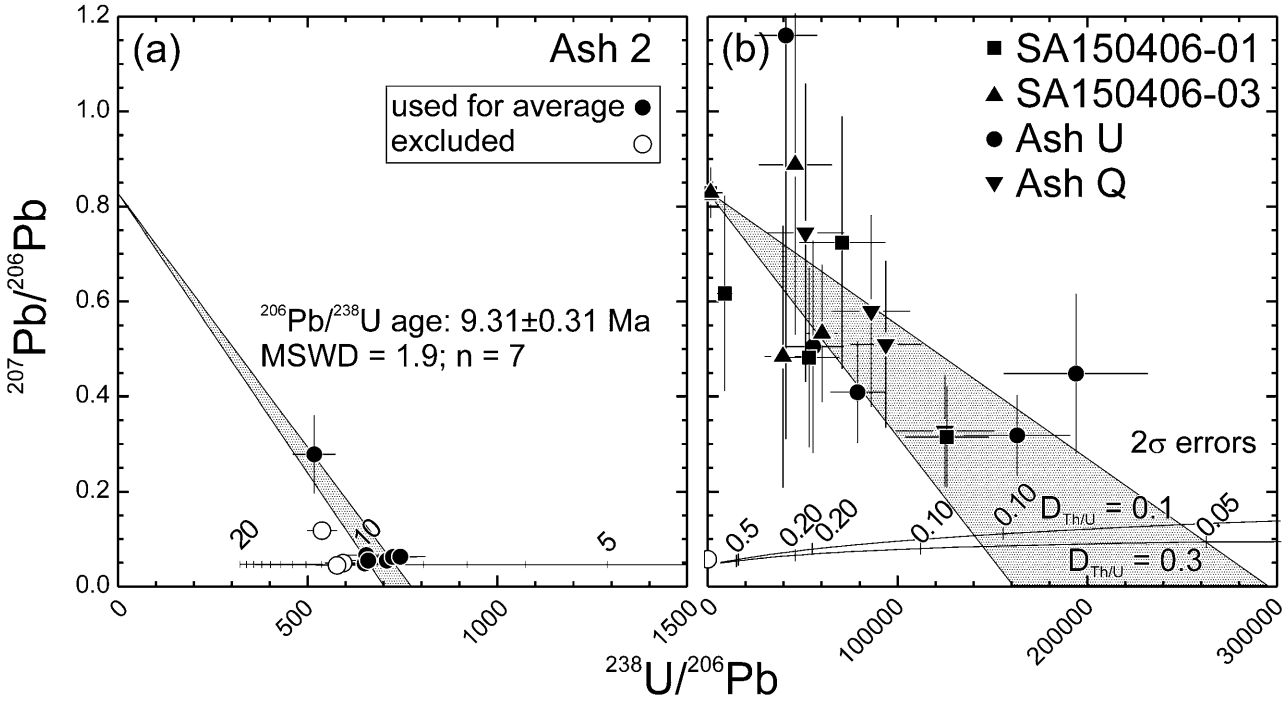

Figure 4. (a and b) Shown are ^{207}Pb/^{206}Pb versus ^{238}U/^{206}Pb zircon results, uncorrected for common Pb, showing segments of Concordia (ages in Ma) and regression lines with a fixed *y* axis intercept corresponding to common Pb (^{207}Pb/^{206}Pb = 0.83). Concordia intercept ages in Figure 4b vary as a function of the fractionation between Th and U in zircon crystallizing from a melt. The ^{206}Pb deficit resulting from ^{230}Th disequilibrium was calculated from zircon mineral melt distribution coefficients ($D_{Th/U}$) between ~0.1 and 0.3, estimated from Th/U in zircon and the average for continental arc magmas. Based on model intercept ages, maximum eruption ages for ashes SA150406-01, SA150406-03, Ash U, and Ash Q of 0.10 ± 0.05 Ma are inferred.

the reproducibility of AS3 zircon (1099.1 Ma [*Paces and Miller*, 1993]) are 2.3%–2.7%. Secular equilibrium standard AS3 yielded (^{230}Th)/(^{238}U) = 1.001 ± 0.013 (MSWD = 0.3; n = 12) with parentheses denoting activities. U-Th zircon melt isochron ages [*Reid et al.*, 1997] were calculated using published (^{230}Th)/(^{232}Th) and (^{238}U)/(^{232}Th) for evolved central Andean lavas (Parinacota rhyolite 91-014 from *Bourdon et al.* [2000]) as representative of the melt. Because of the strong U/Th fractionation of zircon relative to the melt, uncertainties in the melt composition contribute to the overall uncertainty of the model ages only to a negligible amount.

[20] Ash 2 yielded a ^{206}Pb/^{238}U age of 9.31 ± 0.31 Ma (2σ; mean square of weighted deviates MSWD = 1.9; n = 7; Figure 4a). Three zircon crystals in Ash 2 are slightly older (~11 Ma), and were omitted from the average. Ash 3 yielded few crystals, and the ones analyzed are Paleozoic-Precambrian in age (^{206}Pb/^{238}U age between 315 and 711 Ma; n = 4). Because xenocrystic zircon is rare in the other ashes, we interpret these crystals to be detrital. Initial U-Pb dating of zircon crystals in samples Ash U, Ash Q, SA150406-01, and SA150406-03 yielded very low and highly unradiogenic ^{206}Pb intensities. Although individual age uncertainties are large, the zircon crystals have Late Pleistocene ^{206}Pb/^{238}U ages (with an overall average between ~50–120 ka, after correction for initial disequilibrium; Figure 4b), with the exception of a single old zircon (~534 Ma) in Ash U. The young crystallization age of these zircons was confirmed by subsequent ^{238}U-^{230}Th dating which indicated uranium-series disequilibrium in most crystals with (^{230}Th)/(^{238}U) ranging between 0.18 and 1.0. Zircon melt model ages (Figure 5 and Table 2) range between 22 ka and >380 ka (which represents the upper age limit resolvable by the ^{238}U-^{230}Th method). The geochronological data cannot distinguish between crystals being derived from different eruptions, or protracted crystallization within an individual magma system and a single eruption. Protracted zircon crystallization is characteristic for silicic magma systems in convergent margin settings [e.g., *Schmitt et al.*, 2010]. Regardless of the causes for the heterogeneous zircon age population in these ashes, it is the youngest crystal(s) in each population which we use in order to constrain maximum depositional ages (Figure 5): Ash U (22 ± 10 ka), Ash Q (47 ± 6 ka), SA150406-01 (37 ± 6 ka), and SA150406-03 (26 ± 10 ka).

3.2. Paleoflow Reconstructions

[21] To reconstruct paleoflow directions the orientation of individual pebbles (usually 60 or more) in clast-supported conglomerates were measured. Using STEREONET software (Allmendinger; www.geo.cornell.edu/geology/faculty/

Table 1. U-Pb Zircon Results[a]

Sample/Grain	$^{238}U/^{206}Pb$	$^{238}U/^{206}Pb$ 2σ	$^{207}Pb/^{206}Pb$	$^{207}Pb/^{206}Pb$ 2σ	Correlation of Concordia Ellipses	$^{206}Pb/^{238}U$ Age (Ma)	$\pm2\sigma$ (Ma)	U (ppm)	Th (ppm)	UO^+/U^+[b]	Percent ^{206}Pb[c]
Ash 2											
1	744	66	0.0627	0.0145	−0.16	8.56	0.79	270	120	8.5	98
10	660	47	0.0548	0.0082	0.10	9.74	0.71	750	450	8.3	99
2	650	47	0.0487	0.0037	−0.09	9.99	0.71	2,600	360	8.4	100
3	725	62	0.0620	0.0188	0.09	8.77	0.79	380	460	8.5	98
4[d]	577	56	0.0450	0.0050	−0.14	11.3	1.1	940	190	8.0	100
5[d]	593	48	0.0492	0.0044	−0.06	10.9	0.9	1,800	260	8.0	100
6	654	60	0.0666	0.0066	−0.14	9.69	0.92	1,500	320	8.3	97
7[d]	538	40	0.118	0.004	−0.05	10.9	0.9	3,600	4,700	8.1	91
8	517	57	0.278	0.082	−0.53	8.85	2.10	500	290	9.0	70
9	708	55	0.0548	0.0049	0.31	9.10	0.71	1,400	270	8.7	99
Ash Q											
1[e]	163,000	28,000	0.318	0.085	0.30	0.1	0.05	8,500	2,200	8.4	65
2[e]	78,900	14,300	0.409	0.107	0.05	0.1	0.05	3,100	1,200	8.6	54
3[e]	55,600	16,000	0.505	0.224	0.41	0.1	0.05	860	360	8.2	41
4[e]	194,000	38,000	0.448	0.168	0.41	0.1	0.05	6,400	1,400	8.4	49
5[e]	41,100	16,600	1.16	0.85	0.64	0.1	0.05	260	180	8.6	-
Ash U											
1	11.6	0.8	0.0575	0.0008	0.06	534	38	790	70	8.2	100
2[e]	51,500	20,400	0.745	0.314	0.56	0.1	0.05	760	220	8.3	11
3[e]	93,800	18,700	0.510	0.176	0.59	0.1	0.05	3,100	810	8.4	41
4[e]	125,000	26,000	0.328	0.118	0.81	0.1	0.05	6,200	1,800	8.4	64
5[e]	86,100	20,500	0.580	0.202	0.33	0.1	0.05	2,200	490	8.3	32
SA150406-01											
1[e]	70,800	22,800	0.724	0.266	0.34	0.1	0.05	790	580	8.7	13
2[e]	1,080	130	0.828	0.061	0.09	0.1	0.05	490	400	8.4	-
3[e]	126,000	22,000	0.315	0.106	0.31	0.1	0.05	6,400	2,000	8.4	66
4[e]	53,400	15,900	0.482	0.189	0.45	0.1	0.05	820	210	9.5	44
5[e]	9,010	1,900	0.617	0.206	0.34	0.1	0.05	350	260	8.4	27
SA150406-03											
2[e]	60,200	8,400	0.533	0.144	0.65	0.1	0.05	4,000	1,400	8.2	38
3[e]	1,590	240	0.829	0.053	0.02	0.1	0.05	490	410	8.2	-
4[e]	46,100	19,400	0.888	0.358	0.48	0.1	0.05	530	270	8.4	-
5[e]	39,600	9,600	0.484	0.276	0.47	0.1	0.05	800	210	8.3	44

[a]The reproducibility of our standard AS3 [*Paces and Miller*, 1993] (see also our standard) $^{206}Pb/^{238}U$ ages is 1 relative standard deviation 2.7% (n = 36).
[b]UO^+/U^+ calibration range for AS3 between 8.0 and 8.6.
[c]Radiogenic (after ^{207}Pb-based common Pb correction; $^{207}Pb/^{206}Pb$ common = 0.823).
[d]Excluded from average.
[e]Approximate age after disequilibrium correction.

RWA/programs.html) this raw data was then rotated so as to restore bedding to horizontality. According to this procedure clast orientations are assumed to point upstream (i.e., imbrication) requiring 180° rotation around the vertical to reflect transport direction. Figure 6 represents the raw (i.e., unrotated) lower hemisphere projection of the data and the orientation of bedding. The central tendency of the inferred transport directions is shown in Figure 2b.

3.3. Interpretation of Seismic Reflection Data

[22] Three dimensional reflector mapping and analysis was completed on the unmodified (i.e., not depth migrated) data set using Schlumberger Petrel software. We measured the vertical distance (in two-way traveltime (TWT)) of the Cretaceous rift sediments to assess if extensional structures (i.e., localized extensional depocenters) are present in the seismic grid. To illustrate the geometry of the inferred half-graben depocenters we "flattened" the first (i.e., deepest) postrift reflector, which amounts to a purely vertical distortion. This approach is a good approximation of the reflector geometries prior to shortening since the inferred extensional fault did not offset the stratigraphic interval shown. If not noted otherwise, seismic sections are displayed without modifications.

4. Results

4.1. Tectonostratigraphy

[23] In addition to the shortening accommodated by the reactivated former extensional hanging walls now constituting the ranges in the broken foreland, the basins have also been shortened, affecting most of the synorogenic succession [e.g., *Kley and Monaldi*, 2002; *Salfity et al.*, 2004]. In the basins, the Neogene deposits have been folded and faulted by mild inversion of Cretaceous extensional fault systems in both the SBS [*Cristallini et al.*, 1997] and the EC [*Carrera and Muñoz*, 2008]. Below, we present further evidence for Quaternary deformation in the eastern EC and the SBS, making a case for an episode of widespread, continued basin inversion. These intrabasin structures are of particular importance because they create accommodation space for the La Troja Formation. We will demonstrate that large volumes

Table 2. U-Th Zircon Results[a]

Zircon	(^{238}U/^{232}Th)	(^{230}Th/^{232}Th)	Age (ka)	+2σ	−2σ	U (ppm)
		SA150406-01				
1	4.65 ± 0.19	2.95 ± 0.19	91	14	−14	650
2	3.85 ± 0.16	1.63 ± 0.25	37	12	−12	230
3	11.7 ± 0.44	6.30 ± 0.25	78	6	−6	5000
4	9.47 ± 0.40	5.80 ± 0.20	95	10	−8	3300
5	3.81 ± 0.23	1.79 ± 0.33	47	20	−18	260
6	1.58 ± 0.10	0.91 ± 0.11	27	20	−18	360
7	6.05 ± 0.77	5.72 ± 0.70	304	∞	−204	630
8	8.37 ± 0.31	6.13 ± 0.46	134	26	−24	630
9	2.94 ± 0.13	1.30 ± 0.22	33	16	−14	290
10	4.54 ± 0.16	1.85 ± 0.30	38	12	−12	270
11	3.83 ± 0.20	1.85 ± 0.37	49	22	−20	200
12	6.40 ± 0.27	4.74 ± 0.17	134	18	−16	2800
13	5.88 ± 0.37	4.79 ± 0.42	170	58	−46	430
14	3.74 ± 0.15	1.48 ± 0.31	31	16	−14	310
15	2.58 ± 0.18	2.36 ± 0.18	232	172	−94	1000
		SA150406-03				
3	3.50 ± 0.14	1.31 ± 0.21	26	10	−10	360
2	8.31 ± 0.29	4.91 ± 0.22	88	8	−8	2600
4	6.13 ± 0.22	5.31 ± 0.26	206	48	−40	1200
5	8.85 ± 0.61	6.71 ± 0.45	146	36	−30	800
6	6.00 ± 0.29	3.49 ± 0.35	81	18	−16	460
7	10.5 ± 0.51	5.89 ± 0.26	82	10	−8	2700
8	8.40 ± 0.32	3.26 ± 0.77	44	18	−16	200
9	7.15 ± 0.39	6.94 ± 0.48	377	∞	−200	540
10	51.2 ± 2.44	47.95 ± 3.17	299	200	−102	750
11	3.23 ± 0.14	1.52 ± 0.21	42	14	−14	360
12	5.40 ± 0.21	2.76 ± 0.34	63	16	−14	310
13	4.04 ± 0.18	3.70 ± 1.06	248	∞	−206	90
16	6.66 ± 0.30	4.75 ± 0.21	124	18	−16	1900
		Ash Q				
1	6.84 ± 0.27	4.79 ± 0.20	119	14	−14	7900
2	7.88 ± 0.50	5.97 ± 0.34	144	30	−28	990
3	5.23 ± 0.19	3.05 ± 0.24	80	14	−12	700
4	12.6 ± 0.45	7.13 ± 0.22	85	6	−6	4400
5	4.17 ± 0.18	2.08 ± 0.41	55	24	−20	220
6	1.65 ± 0.06	1.00 ± 0.06	38	12	−10	1200
7	3.62 ± 0.13	1.62 ± 0.24	40	14	−14	320
8	2.88 ± 0.11	1.56 ± 0.21	53	18	−16	280
9	3.25 ± 0.15	1.55 ± 0.19	43	12	−12	390
10	12.6 ± 0.44	7.31 ± 0.40	89	10	−10	1400
11	3.82 ± 0.17	2.59 ± 0.32	101	32	−28	330
12	7.84 ± 0.31	4.04 ± 0.50	69	16	−14	620
13	2.93 ± 0.14	1.68 ± 0.22	62	22	−20	320
14	2.85 ± 0.24	2.71 ± 0.18	297	∞	−154	2200
15	7.25 ± 0.28	3.14 ± 0.49	51	14	−12	250
		Ash U				
2	10.1 ± 0.36	6.00 ± 0.54	91	16	−16	560
3	12.5 ± 0.51	7.26 ± 0.30	89	8	−8	2500
4	10.5 ± 0.37	5.73 ± 0.18	78	6	−6	5000
5	11.6 ± 0.58	8.04 ± 0.40	121	18	−16	1700
6	7.80 ± 0.47	4.82 ± 0.50	95	22	−20	560
7	7.97 ± 0.35	5.00 ± 0.19	97	10	−10	3200
8	4.83 ± 0.33	5.12 ± 0.39	∞	∞	∞	560
9	4.79 ± 0.22	1.94 ± 0.28	39	12	−10	370
10	9.33 ± 0.32	5.89 ± 0.32	100	12	−12	1900
11	4.81 ± 0.19	2.46 ± 0.35	60	18	−16	250
12	3.78 ± 0.14	2.04 ± 0.20	61	14	−12	560
13	12.4 ± 0.47	6.67 ± 0.33	78	8	−8	3100
14	2.83 ± 0.10	1.49 ± 0.28	50	24	−22	200
15	9.02 ± 0.63	4.73 ± 0.59	72	18	−16	410
16	5.96 ± 0.29	1.69 ± 0.38	22	10	−10	320

of Quaternary sediments are stored at moderate to high elevation despite drainage connectivity to the foreland.

4.1.1. Coronel Moldes Anticline

[24] A grid of eleven seismic lines from the Coronel Moldes area augmented by borehole data and detailed structural mapping have helped to decipher the deformation history of the basin interior in the Lerma Valley (eastern EC; Figure 2).

[25] A planar 255° (WSW) dipping anisotropy was imaged in the basement below the town of Coronel Moldes (Figure 7). The anisotropy does not displace Neogene strata, nor is it oriented parallel to the 35°–215° (NE-SW) trending Coronel Moldes anticline [*Hain and Strecker*, 2008] (Figure 8e). We tentatively relate this subsurface structure to the N–S striking Precambrian basement structures (i.e., the thrust separating the Choromoro and Lules tectonometamorphic belts, or alternatively, the west dipping axial plane foliation of the Choromoro Belt [see *Mon and Hongn*, 1991]).

[26] Although no normal fault was directly imaged in the investigated seismic sections, the thickness distribution of the Cretaceous rift fill, interpolated from the seismic grid, defines four distinct depocenters (DC1 to DC4 in Figure 8e). Three of the depocenters are aligned within the core of the Coronel Moldes anticline (Figures 8e and 9). Toward the SW, where the DC4 is offset to the west, the anticline abruptly disappears in both surface and subsurface expression. In the area of DC4, a second subparallel anticline has developed. The overall geometry defined by the deformed fills thus resembles a SSW striking, WNW dipping, en echelon half-graben array. The absence of reflector offsets in the synextensional strata (Figure 9) may be related to drape folding [e.g., *Howard and John*, 1997]. Nonetheless, a more complex deformation mechanism involving transtension [e.g., *Janecke et al.*, 1998] of the aforementioned deep basement anisotropy resulting in fault-oblique drape folding cannot be excluded.

[27] The early deformation episode separating the Guanaco Formation and the Metán Subgroup has no expression discernible in our field observations. However, a low-amplitude angular unconformity imaged by the seismic survey (Figure 7) correlates with the transition between the Metán Subgroup and the Guanaco Formation (Figure 8). We suggest that this erosional truncation of Metán Subgroup strata in the eastern EC, onlap relationships in the SBS [e.g., *Cristallini et al.*, 1997], and a new isolated sediment source at the EC/SBS transition (section 4.2.1), reflect the uplift of the Metán Range at ~10 Ma.

[28] Since the Coronel Moldes anticline involves the Piquete Formation (Figure 8) with an intercalated volcanic ash dated at 1.3 ± 0.2 Ma [*Malamud et al.*, 1996], the inversion of the fault array must be younger. During and after folding sedimentation of the La Troja Formation occurred

Notes to Table 2:

[a]Decay constants used are as follows: λ_{230}, $9.1577 \cdot 10^{-6}$ a^{-1}; λ_{232}, $4.9475 \cdot \times 10^{-11}$ a^{-1}; λ_{238}, 1.55125×10^{-10} a^{-1}. Age is calculated from two point isochrons between zircon and melt using Parinacota rhyolite whole-rock compositions (^{230}Th)/(^{232}Th) = 0.724 and (^{238}U)/(^{232}Th) = 0.726 from *Bourdon et al.* [2000] as representative for the melt. All errors reported at 2σ; secular equilibrium is indicated by the infinity symbol.

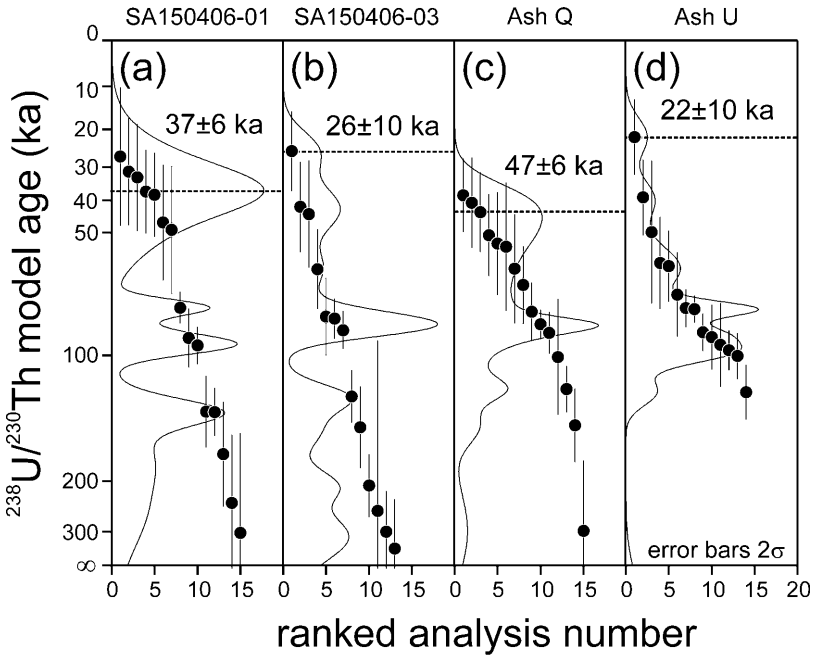

Figure 5. (a–d) Shown are ^{238}U-^{230}Th zircon model ages and relative probabilities plotted for SA150406-01, SA150406-03, Ash Q, and Ash U. Dashed lines indicate maximum depositional age determined from the youngest zircon crystallization age in the population. For sample sites see Figure 2b.

on both sides of the anticline but at different elevations (up to 1400 m to the west and 1130 m to the east) as a result of structurally controlled sediment ponding west of the fold (Figure 8c). Onlap against the anticline is imaged in the seismic reflection profiles (Figure 8b) and can be locally seen in outcrop (Figure 8a). The sediment-filled western syncline exhibits growth strata. Beneath the town of Coronel Moldes (i.e., the filled eastern syncline) the La Troja Formation attains an acoustic thickness of 240 ms (two-way traveltime, TWT) (Figure 7).

[29] The modern topographic expression of the Coronel Moldes fold array may at first sight appear to be minor, especially when compared to the ranges that segment the foreland. Nonetheless, we argue that this Quaternary intrabasin structure absorbed shortening at a high rate. Perpendicular to the structures, the 19.5 km long top of the Piquete Formation was shortened to 16.5 km (Figure 8c). Given the 1.3 ± 0.2 Ma age of the ash intercalated within this unit [*Malamud et al.*, 1996] we find that the strata were shortened at a rate in excess of 3.1 ± 0.6 mm/a.

4.1.2. Sierra Vaqueros and San Lorenzo Anticline

[30] A second example of a Quaternary fold array in the Lerma Valley can be found near the northwestern limits of the city of Salta, the provincial capital (Figure 10). Here, the fault-cored Sierra Vaqueros exposes Piquete Formation conglomerates, and the en echelon San Lorenzo anticline involves Quaternary strata (i.e., the La Troja Formation). The top of the Sierra Vaqueros structure is 700 m higher than the floor of the Lerma Valley. Multiple uplifted fluvial terraces attest to recent deformation and modification of the river network, unambiguously documenting that this structure is actively growing in a southwestward direction. We attribute much of the ~140 m elevation difference between San Lorenzo (1340 m; west of the fold) and Salta (1200 m; east of the fold) to differential Quaternary sediment storage (Figure 10); a situation very similar to the two filled synclines in the Coronel Moldes area (Figure 8c). It is interesting to note that one of the recent earthquakes located within the interior of the Lerma Valley, a magnitude 6.3 event, was registered immediately east of the Sierra Vaqueros (Figure 10; USGS event ID: U.S.2010tfc3).

4.1.3. Santa Barbara System Inversion

[31] Previous studies have shown that Andean contractional structures in the SBS invert Cretaceous normal faults [e.g., *Grier et al.*, 1991; *Cristallini et al.*, 1997; *Kley and Monaldi*, 2002]. Onlap of the Guanaco Formation just east of the Metán Range has been documented [*Cristallini et al.*, 1997], and the Guanaco and Piquete formations are not separated by an angular unconformity [*Cristallini et al.*, 1997; *Gonzalez Villa*, 2002]. Both units, however, have been subsequently folded and faulted (Figure 11) [*Gonzalez Villa*, 2002; *Kley and Monaldi*, 2002]. During and after shortening the Quaternary La Troja sediments were deposited in the synclines; in Figure 11, the east sloping remnant fill surface of the central syncline reaches elevations of >1250 m whereas the fill of the eastern syncline slopes south at elevations well below 1000 m. Possible onlap relationships and/or growth strata in the central syncline have been largely eroded. Along the eastern flank of the Mojotoro Range remnant alluvial fan conglomerates pertaining to the La Troja Formation rest unconformably on the folded and eroded Mio-Pliocene strata (Figure 11). The tectonostratigraphic patterns observed in the SBS therefore resemble those that we have documented in the Coronel Moldes area. Importantly, large volumes of Quaternary sediments are stored at high eleva-

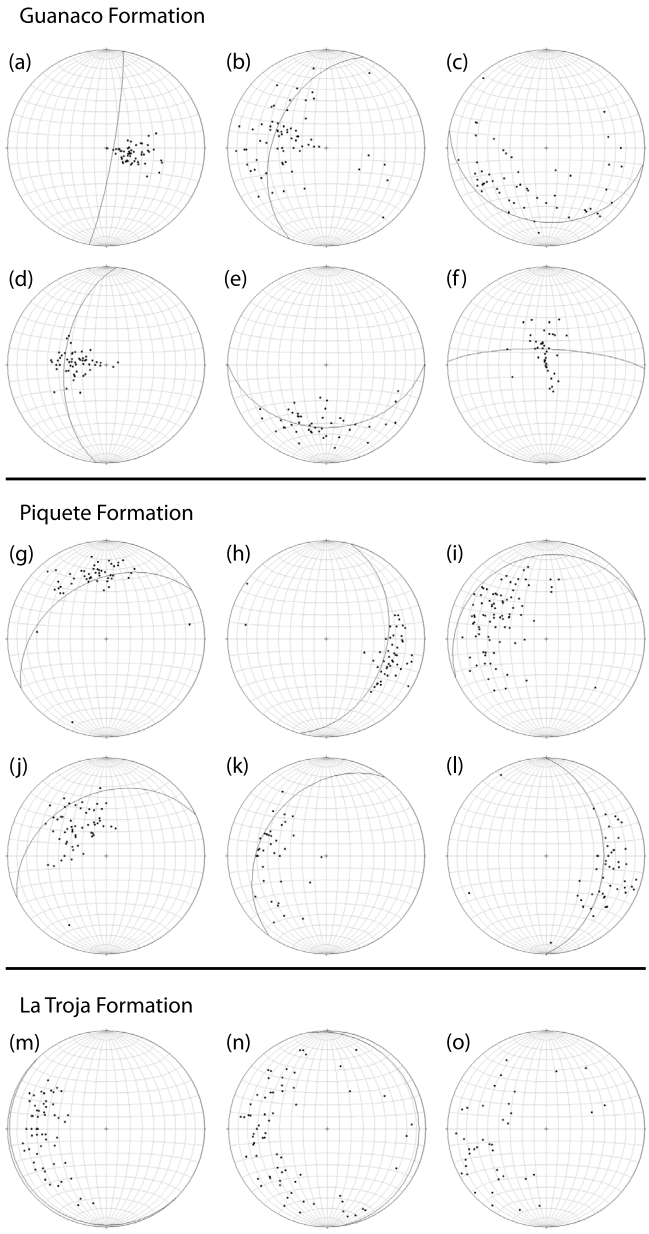

Figure 6. Paleoflow reconstruction based on clast imbrications. Shown here are lower hemisphere projections of clast orientations as measured in the field and bedding orientations (great circle). The central tendency derived from these data (corrected for deformation) is shown in Figure 2b as paleoflow direction; see section 3.2 for details on the correction. The precise locations of the stations are (a) 25°26.062′S, 65°36.617′W; (b) 25°13.888′S, 65°26.232′W; (c) 24°49.606′S, 65°0.824′W; (d) 25°7.739′S, 65°5.485′W; (e) 25°11.941′S, 64°57.335′W; (f) 25°17.334′S, 64°55.652′W; (g) 25°31.602′S, 65°30.682′W; (h) 25°26.659′S, 65°35.448′W; (i) 25°16.142′S, 65°31.955′W; (j) 24°42.654′S, 65°26.922′W; (k) 24°48.019′S, 65°1.484′W; (l) 25°7.833′S, 65°01.206′W; (m) 24°47.363′S, 65°21.440′W; (n) 24°48.103′S, 65°13.353′W; and (o) 25° 13.101′S, 64°56.024′W.

tions and thus contribute to basin average elevation and topographic load.

4.2. Provenance Signatures

[32] Sections 4.2.1–4.2.3 document the composition of conglomerates found in the Guanaco, Piquete and La Troja formations. The changes in clast provenance between these formations speak directly to sediment export versus sediment trapping in the hinterland. We will argue that the disappearance of clasts with a hinterland provenance provides clear evidence for basin-scale trapping of sediments in the intermontane basins.

4.2.1. Guanaco Formation

[33] More than 15% of high-grade metamorphic and granitoid clasts characterize the composition of conglomerates found in the Guanaco Formation in both EC and SBS (Table 3 and Figure 12a), providing a strong constraint for the sediment source areas, as these lithologies only crop out near the Puna margin (Figure 2a). Specifically, in broad agreement with reconstructed paleoflow directions (Figures 2b and 6; see section 3.2), the presence of amphibolites and the leucosome of migmatites indicate eastward sediment transport. Fine-grained, brick red granites of the Tastil pluton (NW of the El Toro lineament outside Figure 2) imply southeastward transport. Thus, our conglomerate composition data (Table 3) identifies the source areas for the Guanaco Formation as the basement ranges to the west of the Palo Pintado Formation depocenter (i.e., ranges at the Puna margin just west of the Calchaquí Valley, western EC). This is important, because it suggests that between ~10 and ~5 Ma sediments were derived from the Puna margin and distributed across the entire foreland.

[34] In addition to the above regional provenance pattern, farther east, in the SBS, the occurrence of hornblende-bearing volcanic, Cretaceous carbonate, and Medina Group basement clasts in Guanaco Formation conglomerates [*Gonzalez Villa*, 2002] (Table 3) suggests a distinct, isolated sediment source. Only the Metán Range at the EC/SBS transition (Figure 2), immediately west of the anomalous Guanaco conglomerates, exposes Medina Group basement, along with the other two lithologies. The Ovejeria Range (Figure 2) also exposes the carbonates and hornblende-bearing volcanic lithologies and can thus not be ruled out as a sediment source during the time of the deposition of the Guanaco Formation (i.e., ~10 to 5 Ma). However, the uplift of the Metán/Ovejeria ranges apparently did not significantly interfere with sediment export from the hinterland.

4.2.2. Piquete Formation

[35] Throughout the eastern EC and SBS, the conglomerate composition of the Piquete Formation dramatically diverges from that of the Guanaco Formation in that plutonic and medium- to high-grade metamorphic clasts are virtually absent (Table 3 and Figure 12a), although most paleoflow indicators within the Piquete Formation show paleoflows toward the E and SE (Figure 2b; note that the south directed flow pertains to the age equivalent San Felipe Formation). Instead, the Piquete Formation composition of conglomerates in the eastern EC and the SBS varies systematically

from N to S, displaying covariance with the location of the El Toro lineament (Figures 12b and 2). This characteristic compositional signal must originate from the ranges (herein central EC) presently separating the Calchaquí Valley in the western EC from the Lerma Valley in the eastern sector of the EC. In contrast to the Piquete Formation, the coeval San Felipe Formation in the Calchaquí Valley retains Guanaco-like conglomerate compositions characterized by plutonic and high-grade metamorphic clasts [*Coutand et al.*, 2006]. The uplift of the central EC ranges must therefore have been able to intercept sediment transport from the Puna margin, causing the divergence between the Piquete and San Felipe conglomerate compositions. This scenario is also compatible with changing transport directions in the San Felipe Formation of the Calchaquí Valley; showing eastward and southward directed paleoflow directions in conglomerates (A. Richter, unpublished data, 2002) (Figure 2b).

[36] Diverging from the above pattern, the Piquete Formation is anomalous at two clast count stations (32 and 34) in the SBS in that it resembles the composition of the Guanaco Formation (Figure 12a and Table 3), suggesting either limited Puna margin sourced sediment bypassing the EC into the SBS or, alternatively, reworking of the Guanaco Formation as observed in the central [e.g., *Gonzalez Villa*, 2002] and eastern parts of the EC.

[37] Notably, in the southernmost Lerma Valley (eastern EC) clast imbrications indicate north directed transport (Station g in Figure 2b). However, the characteristic hornblende-bearing volcanic lithology exposed today in the Ovejeria Range to the south, is absent (clast count station 39).

[38] Overall, the change of conglomerate composition from the Guanaco Formation to the Piquete Formation suggests that between ~5 and 2 Ma coarse sediments shed from the Puna margin were trapped in the intermontane Calchaquí Valley (i.e., the San Felipe Formation, western EC) rather than being exported from the orogen interior. It appears that the uplift of the central EC ranges at ~5 Ma (1) produced the sediment that constitutes the Piquete Formation and (2) intercepted the Puna margin derived gravel.

4.2.3. La Troja Formation

[39] Conglomerate compositions for the Piquete Formation and the La Troja Formation are indistinguishable in the eastern EC except for the decrease in basement clasts and the increased contribution of clasts derived from the Paleozoic and Cretaceous sedimentary cover units to the La Troja Formation conglomerates (relative to Piquete Formation). This difference indicates a shift toward less unroofed sections in the source regions and/or uplift of new sources (Figure 12b) [cf. *Monaldi et al.*, 1996]. In contrast to the Piquete Formation, Pirgua Subgroup sandstones, which disintegrate over very short transport distances in modern rivers, frequently contribute to the La Troja Formation conglomerates in areas proximal to the present-day ranges of the central EC, south of the El Toro lineament.

[40] North of the El Toro lineament, the lithologic contrast between the central EC ranges and the Mojotoro Range is minimal and conglomerate compositions (but not facies; see section 4.3.3) are similar of the Piquete and La Troja formations in both eastern EC and SBS. In the SBS, however, Ordovician fossil-bearing sandstones of the Mojotoro Formation, which are prone to abrasion in modern rivers, contribute to the La Troja Formation, but not to the Piquete Formation, suggesting a marked decrease in transport distance.

[41] At the southern tip of the Mojotoro Range and only few kilometers downstream from the Castillejo Range, the only exposure of black carbonates in the region (Las Tienditas Formation) provides a very direct lithologic constraint (Figure 2a) on the source area for the La Troja Formation in the SBS. While the Guanaco and Piquete formations as well as the base of the exposed section of the La Troja Formation infilling of the local syncline (see section 4.1.3 and Figure 11) are devoid of Las Tienditas clasts (Table 3) [*Gonzalez Villa*, 2002], boulders of the Las Tienditas Formation appear toward the top of the La Troja section, attesting to Quaternary uplift of the Castillejo Range.

[42] In summary, it appears that most of the sediment contributing to the La Troja Formation in the SBS is derived from the ranges at the EC/SBS boundary (i.e., Mojotoro, Castillejo and Metán ranges). Furthermore, there is evidence that large sediment volumes shed from the central EC ranges were trapped by intrabasin structures in the eastern EC (Lerma Valley). The characteristic lithologies exposed along the Puna margin are absent from La Troja Formation conglomerates in both eastern EC and SBS, which indicates that these sediments were efficiently trapped in the western EC (Calchaquí Valley).

4.3. Sediment Dynamics

4.3.1. Guanaco Formation

[43] The geometries of well-defined conglomeratic channels embedded in well-sorted sandstones within the EC and an alternating mudstone-sandstone-conglomerate sequence in the SBS attest to an east-west gradient in the depositional environment. The common provenance signature in Guanaco Formation conglomerates throughout the EC and the SBS (see section 4.2.1 for one exception) with an unambiguous source area near the eastern Puna border suggests a single contiguous depositional system. Strata farther north in the Subandean Belt, characterized by facies relationships similar to those that we document here for the SBS [see also *Gonzalez Villa*, 2002], have been related to a fluvial megafan depositional environment [e.g., *Horton and DeCelles*, 2001; *Leier et al.*, 2005; *Uba et al.*, 2005, 2007, 2009]. The Guanaco Formation may thus also be interpreted as a fluvial megafan;

Figure 7. Interpretation of seismic line 2504, situated in the syncline below the town Coronel Moldes, in the Lerma Valley (eastern EC; see Figure 2b). Depth is shown as seconds of two-way traveltime (TWT). Correlation with the stratigraphic units is based on structural mapping, the nearby borehole CMo.X-1, and seismic facies interpretation. Note the low-amplitude angular unconformity separating the Metán Subgroup from the Guanaco Formation, imaged here as truncation of Metán Subgroup reflectors and the consequent thinning of the Metán Subgroup stratigraphic interval toward the right (NNE). See Figure 8e for location.

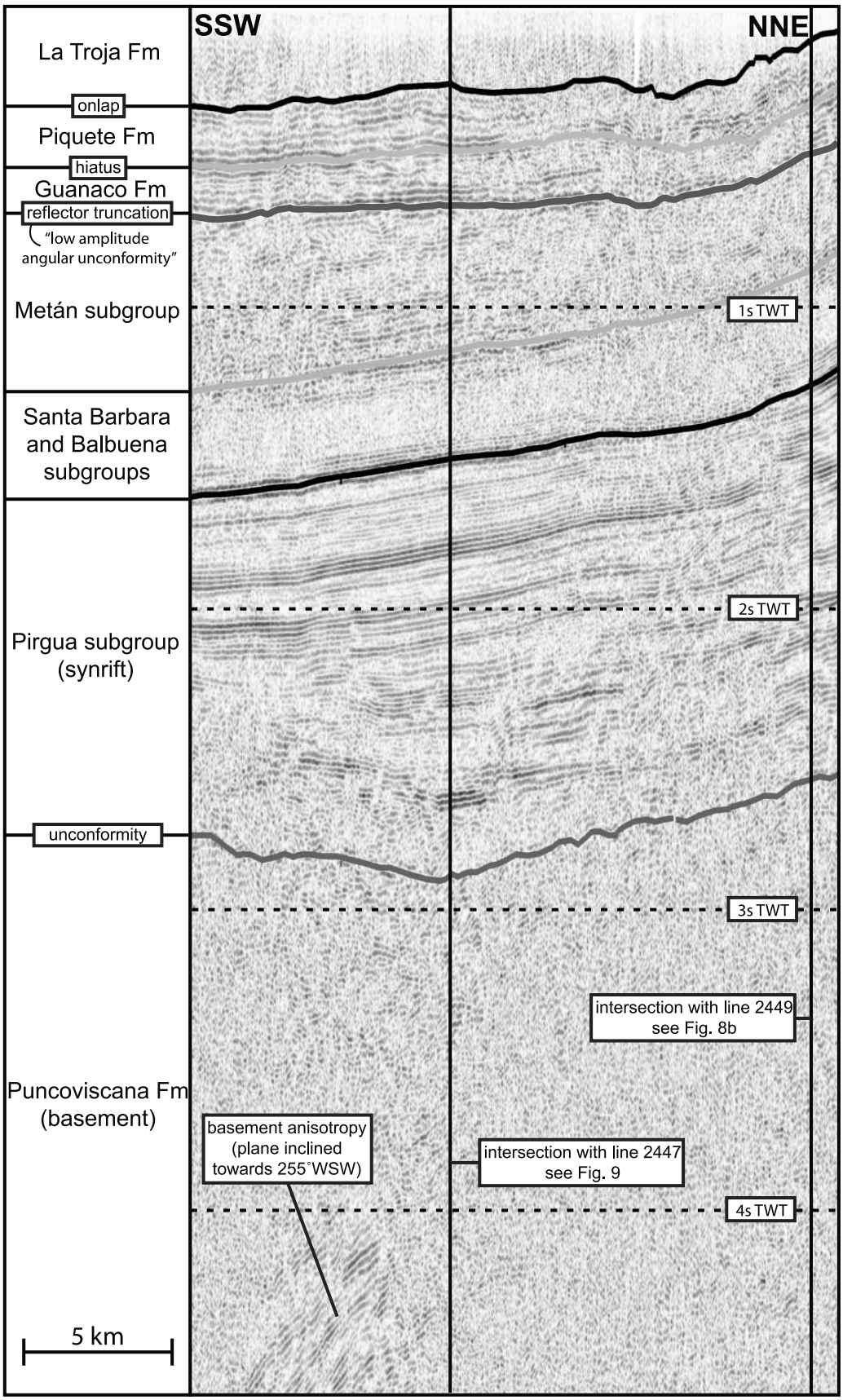
SSW
NNE
La Troja Fm
onlap
Piquete Fm
hiatus
Guanaco Fm
reflector truncation
"low amplitude angular unconformity"
Metán subgroup
Santa Barbara and Balbuena subgroups
Pirgua subgroup (synrift)
unconformity
Puncoviscana Fm (basement)
1s TWT
2s TWT
3s TWT
4s TWT
intersection with line 2449 see Fig. 8b
intersection with line 2447 see Fig. 9
basement anisotropy (plane inclined towards 255°WSW)
5 km

Figure 7

originating along the Puna border and shedding sediment >100 km into the foreland.

4.3.2. Piquete Formation

[44] The characteristic lateral continuity of well imbricated conglomerate horizons in the eastern EC indicates deposition from unconfined flow at relatively high flow velocities, conditions that may be related to an alluvial fan environment below the intersection point [e.g., *Blair and McPherson*, 1994]. Facies associations in the SBS are in accord with distal fan/alluvial plain depositional systems. The central EC provenance signature (see section 4.2.2) is prevalent in both eastern EC and SBS. The Piquete Formation thus appears to be the stratigraphic remnant of a formerly contiguous alluvial fan system, proximal in the eastern EC and distal in the SBS [cf. *Gonzalez Villa*, 2002].

4.3.3. La Troja Formation

[45] The Quaternary La Troja Formation has not been described in detail so far making it timely to document its facies before interpreting the depositional environment and sediment dynamics.

[46] In both eastern EC and SBS, the La Troja Formation comprises poorly stratified and poorly sorted sandy gravels alternating with gravelly sands and clayey sands (see also Figure 8a). The gravels are frequently matrix supported, but clast-supported cobbles exist in channel-like lenses. At some stratigraphic levels occasional boulders are embedded in gravelly sandstones. Siltstones are absent, with the exception of the upper stratigraphic levels of the Coronel Moldes syncline (i.e., west of the Coronel Moldes anticline), where massive banks of friable, chalky, muddy siltstones, containing only rare granules, are associated with infrequent, heavily cemented, longitudinal (i.e., N-S oriented) gravel-filled channels.

[47] The facies associated with the remnant alluvial fan to the east of the Mojotoro Range (Figure 11) are in stark contrast to those described above. Proximal to this range the La Troja Formation is exposed in vertical walls of fanglomerate with no discernible bedding, many tens of meters high (e.g., clast count station 19). The remnant fan surface slopes to the east and east sloping bedding, defined by alternating banks of gravelly sands and sandy gravels, becomes progressively better developed toward the toe of the fan. A massive fanglomerate outcrop, similar to the proximal Mojotoro fan, can be found in the eastern EC near Talapampa (clast count station 21). Here, gravel clasts are dominated by the peculiar hornblende-bearing volcanic lithology deriving from outcrops less than 10 km to the south.

[48] Based on these observations, the depositional environment of the La Troja Formation is best described as proximal alluvial fan systems that developed where streams exit the different range fronts. The transition from proximal fanglomerates to more distal conglomerate/sandstone strata reflects fluvial processing on the fan surface. These fan systems are also affected by the deformation of the basin interior of both the eastern EC and the SBS; large volumes of the La Troja Formation sediments are accommodated by synclines that formed during deposition. The poor sorting and poorly developed bedding of the La Troja sediments filling these synclines may be attributed to the dominance of gravity flow, rather than fluvial, sediment transport mechanisms. It appears that La Troja sediments have not been transported far, but instead were stored adjacent to the various sediment source regions. The facies and provenance signatures of these deposits are thus characterized by pronounced spatial heterogeneity.

4.4. Moisture Supply to the Eastern Flanks of the Andean Orogen

[49] Previous studies have highlighted the tectonic fragmentation and progressive aridification of the Andean hinterland in the immediate vicinity of the Puna as a driver of sedimentary processes and sustained severed drainage conditions in intermontane basins [e.g., *Starck and Anzótegui*, 2001; *Kleinert and Strecker*, 2001; *Sobel and Strecker*, 2003; *Sobel et al.*, 2003; *Alonso et al.*, 2006; *Coutand et al.*, 2006; *Strecker et al.*, 2007a, 2007b]. A detailed account of the present-day geomorphic conditions and related climate patterns for the broken Salta foreland are provided below, and two major controls on moisture supply to the hinterland are identified.

[50] The first of these controls is related to the updraft of air caused by the atmospheric gravity wave that is generated when wind passes over a mountain range [e.g., *Roe*, 2005, and references therein]. This density wave causes higher precipitation on the windward slope than on the leeward slope, where the density wave causes downdraft of the air and thus a rain shadow. Such asymmetric precipitation patterns, with higher precipitation on the eastern slopes, intercepting easterly and northeasterly moisture-bearing winds [e.g., *Vera et al.*, 2006a, 2006b; *Bookhagen and Strecker*, 2008], occur along all ranges in the broken Salta foreland (Figures 13 and 14). However, our data suggests that ranges only reduce downwind rainfall significantly if they surpass a 3 km radius relief of ~1 km (i.e., central EC, Aconquija, Quilmes ranges and the eastern Puna border; Figure 14). A relief threshold of this type is well founded in theoretical considerations and numerical simulations by *Galewsky*

Figure 8. Relationship between Cretaceous extensional structures and Quaternary compressional structures in the eastern EC (Lerma Valley); see Figure 2a for location. (a, b) Onlap relationships of the La Troja Formation indicate that shortening occurred only after deposition of the Piquete Formation. (c) Geologic section across intrabasin structures near Coronel Moldes based on structural mapping, borehole data, and seismic interpretation. (d) The seismic grid is situated within the Cretaceous Salta Rift. (e) The thickness of the synrift stratigraphic interval is characterized by four distinct depocenters (DC 1 to 4). The close correlation between the compressive structures mapped in the field and the acoustic thickness (contoured here as milliseconds two-way traveltime (TWT)) of the rift fill requires inversion of the en echelon array of Cretaceous extensional structures during shortening. The exposed onlap (Figure 8a) is visible along the Tajamar stream, near La Viña, about 20 km SSW of the geologic section (paleoflow station (h) in Figure 2b).

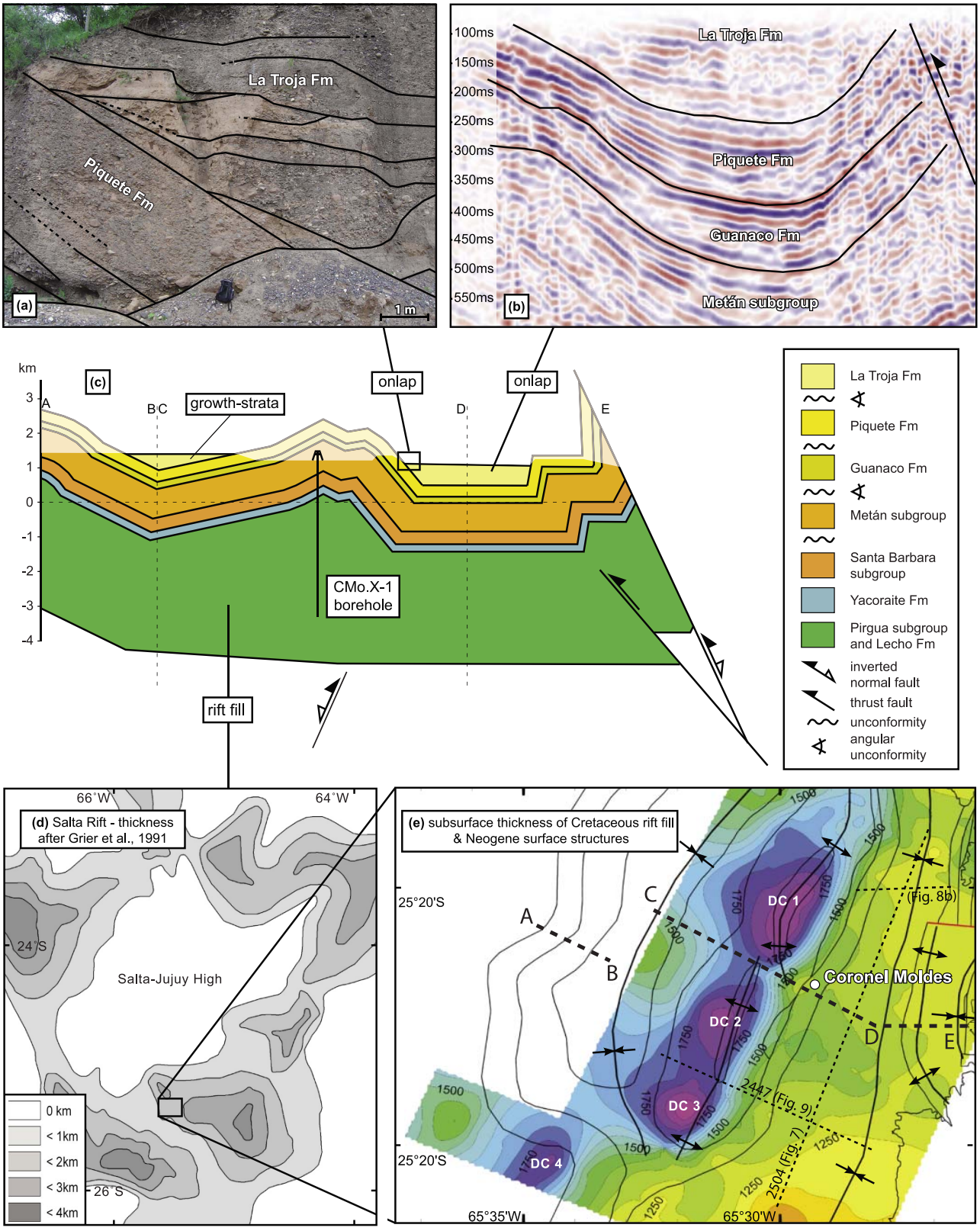
La Troja Fm
Piquete Fm
(a)
1 m
100ms
150ms
200ms
250ms
300ms
350ms
400ms
450ms
500ms
550ms
La Troja Fm
Piquete Fm
Guanaco Fm
Metán subgroup
(b)
km
(c)
A
B
C
D
E
growth-strata
onlap
onlap
CMo.X-1 borehole
rift fill
La Troja Fm
Piquete Fm
Guanaco Fm
Metán subgroup
Santa Barbara subgroup
Yacoraite Fm
Pirgua subgroup and Lecho Fm
inverted normal fault
thrust fault
unconformity
angular unconformity
66°W
64°W
(d) Salta Rift - thickness after Grier et al., 1991
24°S
26°S
Salta-Jujuy High
0 km
< 1km
< 2km
< 3km
< 4km
(e) subsurface thickness of Cretaceous rift fill & Neogene surface structures
25°20'S
65°35'W
65°30'W
DC 1
DC 2
DC 3
DC 4
Coronel Moldes
(Fig. 8b)
2447 (Fig. 9)
2504 (Fig. 7)

Figure 8

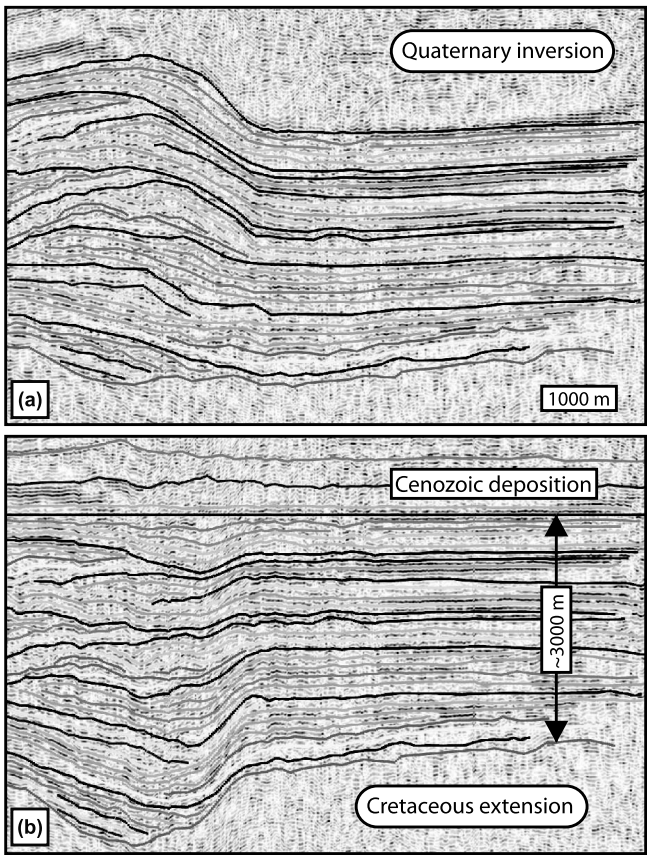

Figure 9. Synrift depth interval of seismic line 2447 across the Coronel Moldes anticline (a) as imaged by the survey and (b) flattened along the oldest postrift reflector. The synrift depocenter in Figure 9b occupies the core of the Coronel Moldes anticline (Figure 9a). Neither the extensional fault nor the blind reverse fault that folds the synorogenic strata was imaged in the seismic data, suggesting drape folding during both extension and compression. See Figure 8e for location.

[2009]. If the scale height (h) of a range increases relative to some measure of atmospheric conditions (i.e., U/N; U = horizontal wind speed; N = atmospheric buoyancy frequency) a regime change of the precipitation patterns causes hinterland aridification, rather than merely reduced precipitation on the lee slope of the range [*Galewsky*, 2009]. Here it is shown that if ranges surpass this relief threshold, but do not completely shield the basins in their lee (i.e., Metán and Candelaria ranges partly shield the Lerma and Rosario valleys; Figures 13 and 14), moisture can pass into these basins where relief is low. Thus, although the Mojotoro range causes orographic precipitation, the low relief of this range allows moisture to penetrate into the Lerma Valley (swath 1 in Figure 14) and consequently into the lee of the high-relief Metán range (swath 2 in Figure 14; see also Figure 13). On longer time scales lateral and vertical fault growth along uplifting ranges will thus promote topographic growth and accrue relief, ultimately resulting in an efficient moisture barrier. In such a setting, moisture transport farther into the orogen interior is limited to thoroughfares formed by areas of reduced relief. Such thoroughfares may be associated with areas where mountain-bounding faults lose throw or where transfer structures have facilitated the exit of major drainages, fluvial downcutting, and valley formation [e.g., *Strecker and Marrett*, 1999; *Strecker et al.*, 2007a] (Figure 13b).

[51] The second factor controlling moisture supply to the hinterland is related to thermodynamics rather than prevailing easterly wind directions. The Clausius-Clapeyron relation governs that the moisture content of the air column decreases with surface temperature/elevation [e.g., *Holton*, 1992; *Roe et al.*, 2002]. The consequence of this relation is apparent in our data when considering the elevation of basins and throughfares, rather than range elevation. Once basin elevations have reached ~1500 to 2000 m (transition from green to yellow colors in Figure 2b), the amount

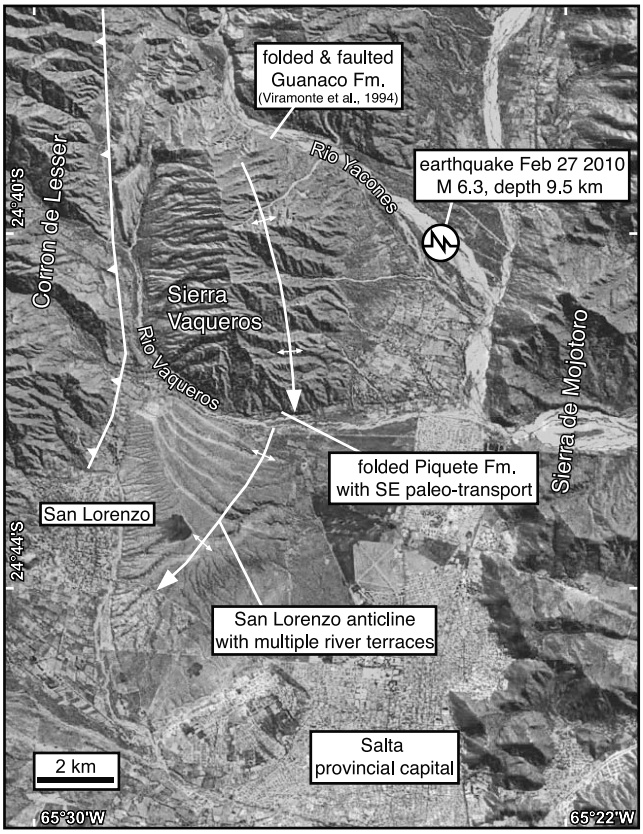

Figure 10. SRTM-enhanced Landsat image with structural interpretation of the Sierra de Vaqueros and San Lorenzo anticline (SRTM data, U.S. Geological Survey); see Figure 2a for location. While the Guanaco and Piquete formations are folded in the Sierra de Vaqueros, the San Lorenzo anticline plunges SSW into the Lerma Valley, also folding the conglomeratic fill (La Troja Formation). A series of incised river terraces record active southward growth of the structural array and the associated reorganization of the fluvial network. The symbol to the east of the Sierra Vaqueros marks the epicenter of a recent magnitude 6.3 earthquake, further attesting to ongoing deformation.

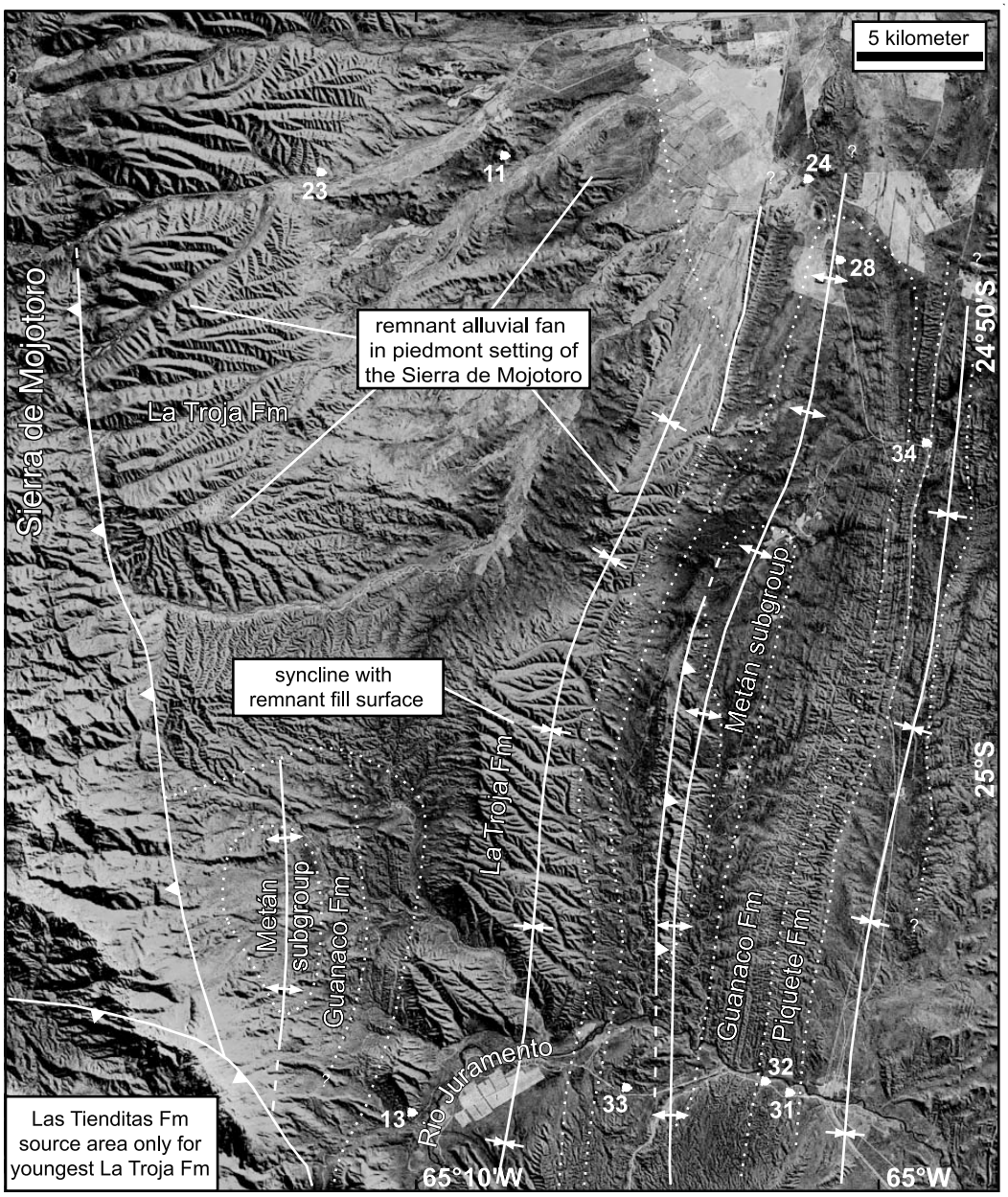

Figure 11. SRTM-enhanced Landsat image with structural interpretation of the SBS, east of the Mojotoro Range (SRTM data from U.S. Geological Survey). See Figure 2a for location. The La Troja Formation is preserved as remnant alluvial fan surfaces and constitutes the infill of the synclines. White points correspond to conglomerate clast count stations, which are labeled as in Table 3.

of rainfall decreases drastically (Figures 13 and 14) under present-day climatic conditions (i.e., at modern atmospheric lapse rates). For example, between the Santa Maria Valley (swath 3 in Figure 14; basin elevation of ~1600 m) and the Calchaquí Valley (basin elevation at ~1900 m and higher; Figure 2b) the amount of precipitation decreases from ~0.5 m/yr to <0.25 m/yr. This observation strikingly resembles the "Clausius-Clapeyron only" model scenario of *Roe et al.* [2002]. Furthermore, these authors document a feedback between reduced uphill precipitation and steady state river profiles (in their case driven by tectonic uplift). In the Salta foreland, however, we documented above that the elevation difference between neighboring basins or even neighboring depocenters within one basin may also increase due to upstream sediment trapping. Thus, reduced precipitation at higher elevation reduces the efficiency of fluvial incision processes and thus promotes sediment trapping [i.e., *Sobel et al.*, 2003], which raises upstream basin elevation and thus further reduces precipitation. This constitutes a positive feedback.

[52] One additional, potentially important interaction between intermontane sediment storage and precipitation

Table 3. Conglomerate Compositional Data

						Puna Border					Paleozoic		Rift Fill			EC/SBS Border		
Station	Formation	Lat. (°S)	Lon. (°W)	N	Basement Greenschist	Plutonic	Metamorphic[a]	Migmatite/ Pegmatite	Tastil Granite	Quartz	Sandstone (Quartz Arenite)	Sandstone (Miscellaneous Lithic)	Red Sandstone (Lithic)	Basalts	White Carbonates	Black Carbonates	Volcanic	Miscellaneous
3	stream	25.3113	65.4929	110	93	0	0	0	0	0	0	7	0	0	9	0	0	1
5	stream	25.3487	65.527	100	90	0	0	0	0	0	0	2	0	0	8	0	0	0
7	stream	25.2837	65.4809	104	80	0	1	0	0	0	0	8	2	0	13	0	0	0
15	stream	25.3353	64.9363	100	85[b]	0	0	0	0	0	3	8	0	0	0	4	0	0
18	stream	25.0509	65.1969	113	21	0	0	0	0	1	74	5	2	0	1	9	0	0
20	stream	24.6861	65.2895	110	18	0	0	0	0	2	63	25	2	0	0	0	0	0
22	stream	25.5769	65.5698	100	51	5	6	0	0	1	0	8	17	7	1	0	4	0
27	stream	25.6371	65.4857	134	77[b]	0	0	0	0	0	0	54	2	1	0	0	0	0
35	stream	25.4502	65.5629	112	100	0	0	0	0	0	1	3	3	0	5	0	0	0
42	stream	25.6234	65.6107	109	59	0	0	0	0	0	0	0	27	6	14	0	3	0
43	stream	25.6308	65.6303	117	48	20	0	0	0	0	0	0	49	0	0	0	0	0
1	La Troja	25.2713	65.5423	72	48	0	0	0	0	0	0	0	9	0	12	0	0	3
4	La Troja	25.265	65.5454	109	73	0	0	0	0	0	0	1	4	1	28	0	0	2
11	La Troja	24.7898	65.1225	108	7	0	0	0	0	1	80	17	0	0	0	0	0	3
13	La Troja	25.0976	65.1696	100	6	0	0	0	0	0	70	1	7	0	16	0	0	0
19	La Troja	24.705	65.2451	103	1	0	0	0	0	0	35	67	0	0	0	0	0	0
21	La Troja	25.5775	65.5696	140	0	0	0	0	0	0	0	11	2	1	7	0	119	0
23	La Troja	24.8017	65.2226	76	0	0	0	0	0	0	53	23	0	0	0	0	0	0
30	La Troja	24.7894	65.3573	100	0	0	0	0	0	0	0	100	0	0	0	0	0	0
38	La Troja	25.4443	65.5908	93	85	0	0	0	0	0	0	1	1	0	6	0	0	0
40	La Troja	25.5206	65.5043	107	87	2	1	2	0	0	2	9	1	0	2	0	1	0
2	Piquete	25.3466	65.5437	100	89	1	0	0	0	0	0	5	0	1	4	0	0	0
9	Piquete	25.237	65.4626	100	69	0	0	0	0	0	0	2	5	0	24	0	0	0
10	Piquete	25.269	65.5326	100	82	0	0	0	0	0	0	2	1	0	15	0	0	0
24	Piquete	24.8003	65.0247	85	46	0	0	0	0	0	33	6	0	0	0	0	0	0
29	Piquete	24.7109	65.4487	135	36	0	0	0	0	0	98	1	0	0	0	0	0	0
31	Piquete	25.1306	65.0201	119	92	3	0	1	0	0	12	4	0	0	6	0	1	0
32	Piquete	25.1294	65.0277	112	87	1	1	0	0	0	8	1	0	0	5	0	9	0
34	Piquete	24.8958	64.9817	110	65	13	2	2	1	0	22	2	0	0	3	0	0	0
37	Piquete	25.4443	65.5908	108	105	0	0	0	0	0	0	0	0	0	3	0	0	0
39	Piquete	25.5267	65.5114	100	86	0	0	0	0	0	1	13	0	0	0	0	0	0
41	Piquete	25.3094	65.4977	119	110	0	0	0	0	0	0	1	0	0	8	0	0	0
6	Guanaco	25.2889	65.4397	50	20	1	0	0	0	0	1	1	0	2	21	0	3	1
8	Guanaco	25.2315	65.4372	75	41	7	14	0	0	3	0	3	0	0	1	0	4	2
12	Guanaco	25.289	64.9276	60	44[b]	7	0	0	0	4	0	0	0	0	0	0	3	2
26	Guanaco	25.199	64.9556	108	55[b]	2	5	7	0	0	20	10	0	0	0	0	9	0
28	Guanaco	24.8268	65.0137	109	38	8	1	12	0	13	11	21	0	0	0	0	5	0
33	Guanaco	25.129	65.0914	110	53[b]	7	1	0	4	0	33	9	0	0	0	0	3	0
36	Guanaco	25.4368	65.6036	118	80	14	4	10	0	0	9	1	0	0	0	0	0	0

[a]Greater than greenschist metamorphic grade.
[b]Recrystalized (i.e., Medina Formation).

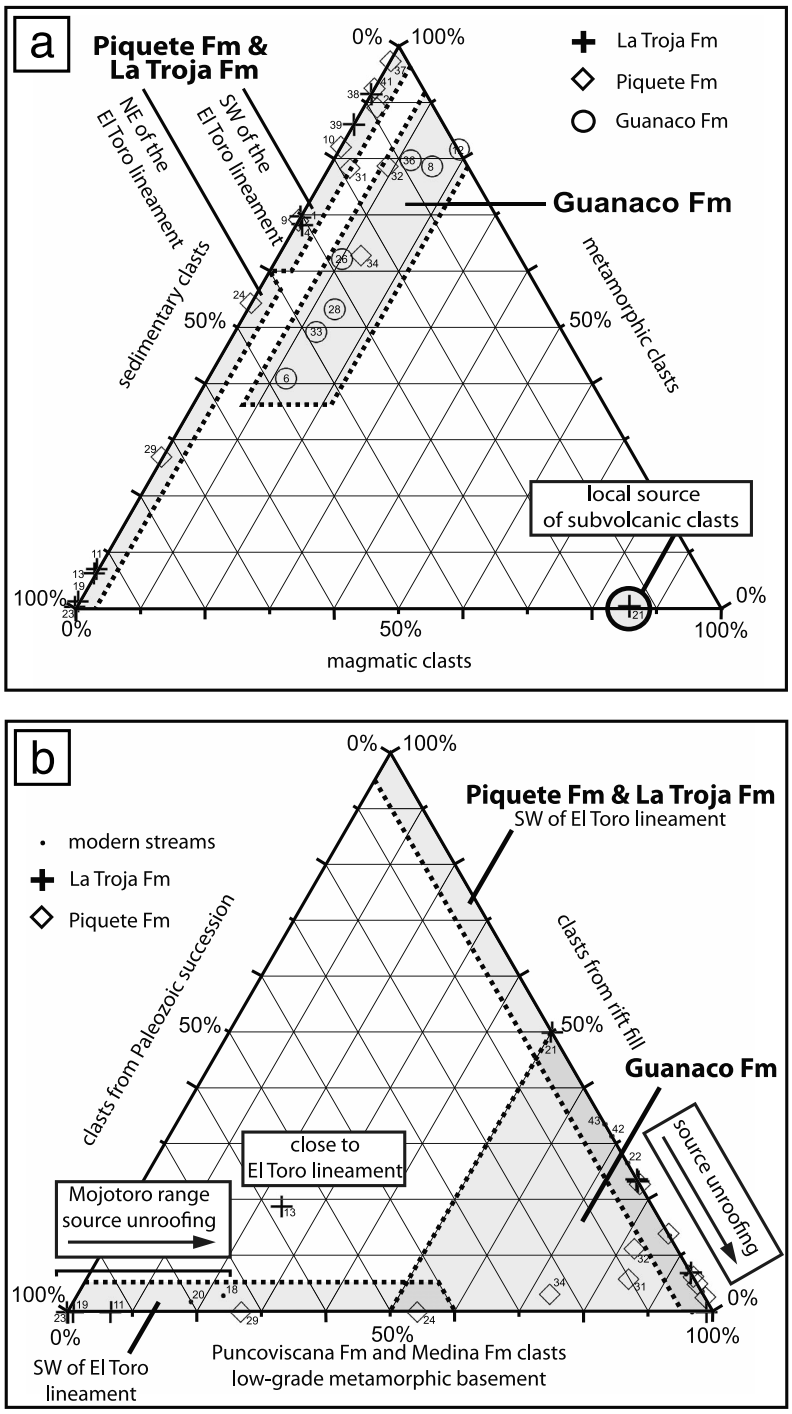

Figure 12. Conglomerate composition and provenance signatures. (a) Guanaco Formation conglomerates are distinguishable from those of the Piquete and La Troja formations on the basis of the contribution of plutonic clasts with a Puna border provenance (the difference between Puna border derived high-grade metamorphic clasts and low-grade metamorphic Puncoviscana basement is not resolved here; this difference would make the Guanco conglomerates even more distinct). (b) Piquete and La Troja formation conglomerates covary with the position of the El Toro lineament of the central EC ranges (see section 4.2). La Troja Formation conglomerates tend to contain proportionally more clasts from synrift (i.e., Cretaceous) or Paleozoic sedimentary cover than do Piquete Formation conglomerates or modern streambed loads, which we interpret as indicating range/source uplift followed by progressive unroofing. Clast count stations labeled as in Table 3. For details on the provenance of the La Troja Formation and specific marker lithologies found therein, see sections 4.2.3 and 2, respectively.

may operate in the Puna plateau where long-term internal drainage conditions have resulted in essentially completely sediment-filled basins [e.g., *Alonso et al.*, 1991; *Vandervoort et al.*, 1995; *Allmendinger et al.*, 1997]. The trapped sediment reduces the basin-to-range elevation difference and thus covers tectonically created relief (Figure 13) [e.g., *Sobel et al.*, 2003; *Strecker et al.*, 2009]. One may speculate that the below-threshold internal relief of the plateau prevents orographic rainout related to the atmospheric gravity wave updraft at the 4–5 km high ranges shown in Figure 14.

5. Discussion

[53] Our records from the Salta foreland include all important elements and characteristics of the complex history of broken foreland systems. In addition, our analysis provides insight into the conspiring role of tectonics and climate in determining the temporally and spatially disparate evolution of sedimentary basins in this environment. Both aspects are discussed below in greater detail.

5.1. Tectonic Fragmentation of the Foreland Basin

[54] The restricted marine Anta Formation deposited during the Miocene Paranense transgression [*Ramos and Alonso*, 1995; *Hernández et al.*, 2005] provides an important timeline during which the foreland system was still a contiguous entity with little relief (Figure 15d). The eastern Puna margin was the sediment source for the strata constituting the Angastaco and Palo Pintado formations of the westernmost EC, which were deposited in an unrestricted foreland [*Díaz and Malizzia*, 1984; *Starck and Anzótegui*, 2001; *Coutand et al.*, 2006]. However, during that time the establishment of internal drainage on the Puna Plateau was underway [e.g., *Alonso et al.*, 1991; *Vandervoort et al.*, 1995]. Tectonism in the western EC [*Coutand et al.*, 2006; *Deeken et al.*, 2006] and a transition to more moist conditions [*Starck and Anzótegui*, 2001] led to facies-belt progradation toward the foreland, establishing the upward coarsening and thickening trend during the deposition of the Metán Subgroup and the Guanaco Formation (Figure 3). The transition between the Metán and Jujuy subgroups in the eastern EC and SBS is marked by the uplift of the Durazno, Runno, and Negro ranges in the western EC (~13 Ma [*Coutand et al.*, 2006]), and the Metán Range (and potentially the Ovejeria Range) at the EC/SBS transition [*Cristallini et al.*, 1997; *Gonzalez Villa*, 2002; *Hain*, 2008; *Strecker et al.*, 2009] (Figure 15c). These events may correlate with the establishment of the low-amplitude angular unconformity in the Lerma Valley (Figure 7). The difference in preserved thickness of the coeval Guanaco Formation between the eastern EC (0–900 m) and the SBS (>2000 m) [*Gebhard et al.*, 1974; *Vergani and Starck*, 1988, 1989a; *Gonzalez Villa*, 2002] potentially reflects this deformation episode, which may have been accompanied by the coalescence of localized depocenters adjacent to the uplifting basement ranges. The areally extensive Guanaco Formation megafan deposits derived from the Puna margin signify an essentially contiguous depositional system. The partitioning of deformation between the far western EC (along the Puna margin) [i.e., *Coutand et al.*, 2006] and the uplift of an isolated sediment source at the EC/SBS boundary (i.e., Sierra de Metán) [*Hain*, 2008; *Strecker et al.*, 2009] (also this study) constitutes a highly disparate pattern of deformation at ~10 Ma (Figure 15c).

[55] Significant compartmentalization of the foreland basin system occurred with the uplift of the central EC ranges at ~5 Ma, which altered three important aspects of the basin characteristics and surface process dynamics (Figure 15b): (1) the EC was segmented into a western and an eastern depozone (the Calchaquí and Lerma valleys, respectively), (2) the conglomerate compositions of the coeval Piquete (eastern EC and SBS) and San Felipe formations (western EC) differ considerably, as sediment export from the western EC became restricted or eventually ceased entirely, and (3) the uplifted ranges of the central EC eventually acted as an efficient orographic barrier causing aridification and transient internal drainage, or at least reduced fluvial connectivity between the leeward intermontane basins in the western EC and the foreland [*Coutand et al.*, 2006]. However, the Sierra de Mojotoro (Figures 2, 10, and 11) had apparently not yet been uplifted at that time and the fluvial systems that drained the eastern EC (i.e., Piquete fans; Figure 15b) were unrestricted and remained connected with and exported sediment to the SBS.

[56] Our new data helps identify the regional pattern of early Pliocene foreland fragmentation of the northern Sierras Pampeanas and the EC, but notably not the SBS. The contact between the Palo Pintado and the San Felipe formations, established as slightly younger than 5.27 ± 0.28 Ma [*Coutand et al.*, 2006] in the transition between the western EC and the Sierras Pampeanas, corresponds to magnetic reversal stratigraphic constraints on the transition between the Guanaco and Piquete formations in the eastern EC at <~6.9 Ma [*Viramonte et al.*, 1994; *Reynolds et al.*, 2000] and the SBS at ~5 Ma [*Reynolds et al.*, 1994, 2000]. Moreover, in the northern Sierras Pampeanas uplift of the Aconquija and Calchaquíes ranges after 6 Ma [*Sobel and Strecker*, 2003], and of the Sierra de Quilmes after 5.4 Ma [*Mortimer et al.*, 2007], are broadly coeval with fragmentation of the Salta foreland. Within the western EC, folding and subsequent erosion of the San Felipe Formation in the northern Calchaquí Valley took place before 2.4 Ma, as evidenced by a pyroclastic deposit that overlies paleotopography sculpted into the San Felipe Formation north of the town of Angastaco; these deposits are in turn overlain by Quaternary alluvial fan conglomerates [*Strecker et al.*, 2007a]. Similarly, in the Santa María basin to the south the entire

Figure 13. (a) Topographic relief within a 3 km radius and (b) Tropical Rainfall Measurement Mission (TRMM) mean annual rainfall. TRMM data is averaged over 12 years (1998 to 2009) and processing methodology is described by *Bookhagen and Strecker* [2008] and *Bookhagen and Burbank* [2010]. Black rectangles outline swath profile locations. White rectangle outlines the location of Figure 2. The eastern border of the internally drained Altiplano-Puna Plateau is marked by the dashed white line; the width of rivers is scaled by drainage area.

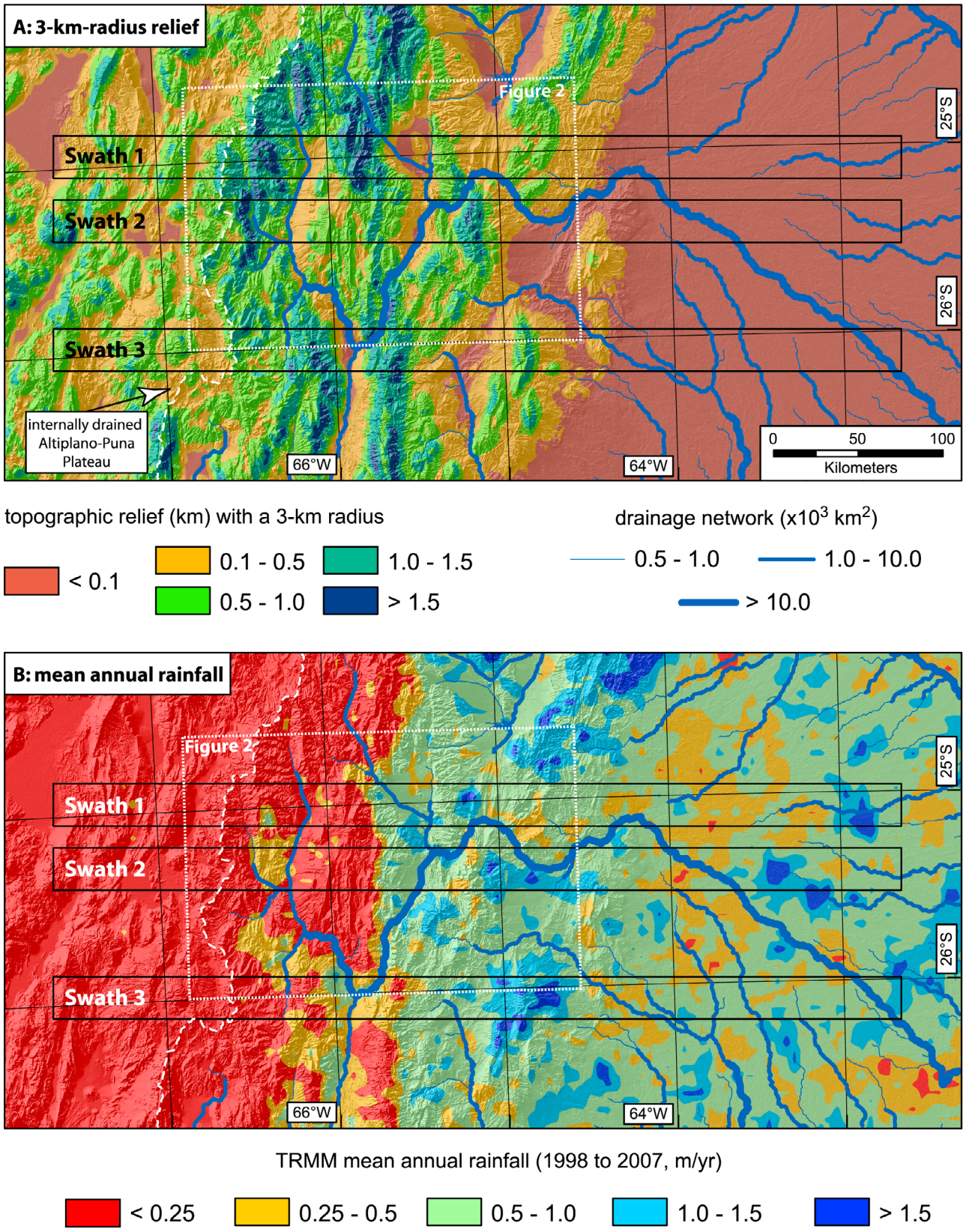
A: 3-km-radius relief
Figure 2
Swath 1
Swath 2
Swath 3
internally drained Altiplano-Puna Plateau
66°W
64°W
25°S
26°S
0 50 100
Kilometers
topographic relief (km) with a 3-km radius
< 0.1
0.1 - 0.5
0.5 - 1.0
1.0 - 1.5
> 1.5
drainage network (x10^3 km^2)
0.5 - 1.0
1.0 - 10.0
> 10.0
B: mean annual rainfall
Figure 2
Swath 1
Swath 2
Swath 3
66°W
64°W
25°S
26°S
TRMM mean annual rainfall (1998 to 2007, m/yr)
< 0.25
0.25 - 0.5
0.5 - 1.0
1.0 - 1.5
> 1.5

Figure 13

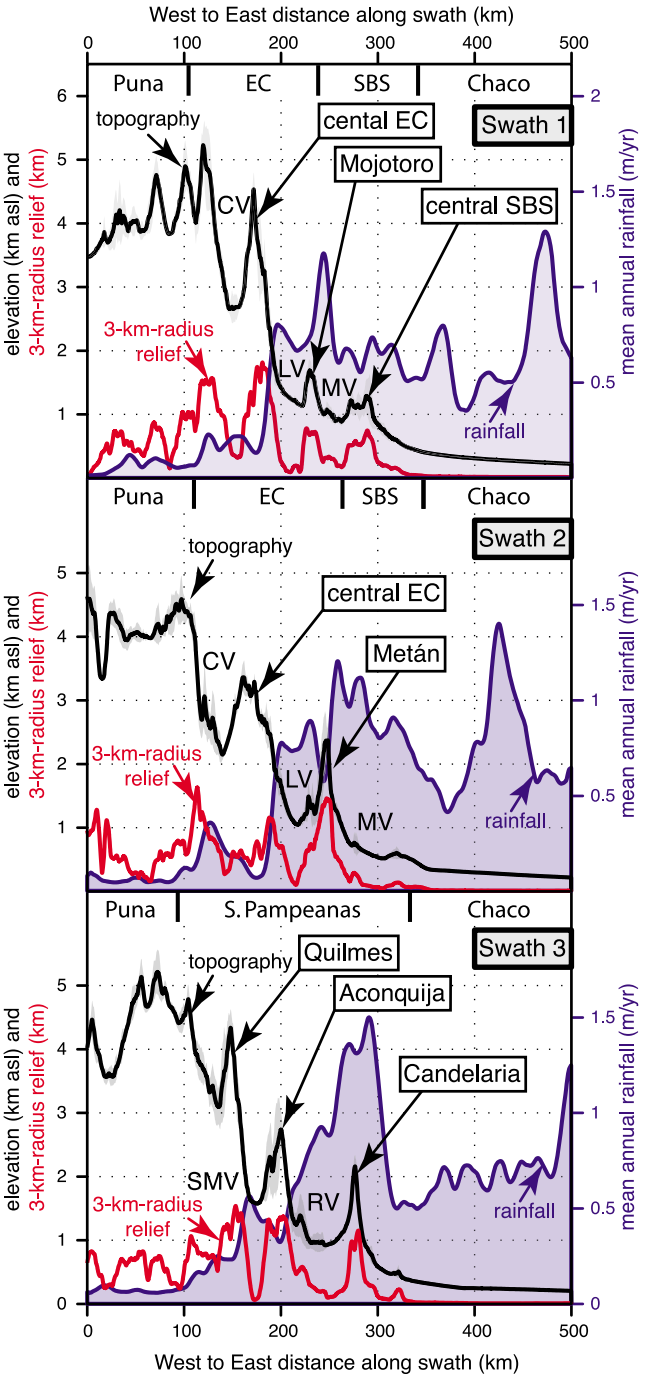

Figure 14. Topography (black), 3 km radius relief (red), and rainfall (blue) swath profiles; see Figure 13 for swath locations. Swaths are 50 km (10 rainfall pixels) wide and 500 km long. Note the relationship between elevation, relief, and rainfall: in the northern swath (swath 1), the moderate elevation and low relief of Mojotoro Range does not result in an efficient moisture barrier. However, Aconquija Range in swath 3, with an elevation >2700 m and laterally continuous high relief, is an efficient orographic barrier. CV, Calchaquí Valley; LV, Lerma Valley; MV, Metán Valley; SMV, Santa Maria Valley; RV, Rosario Valley.

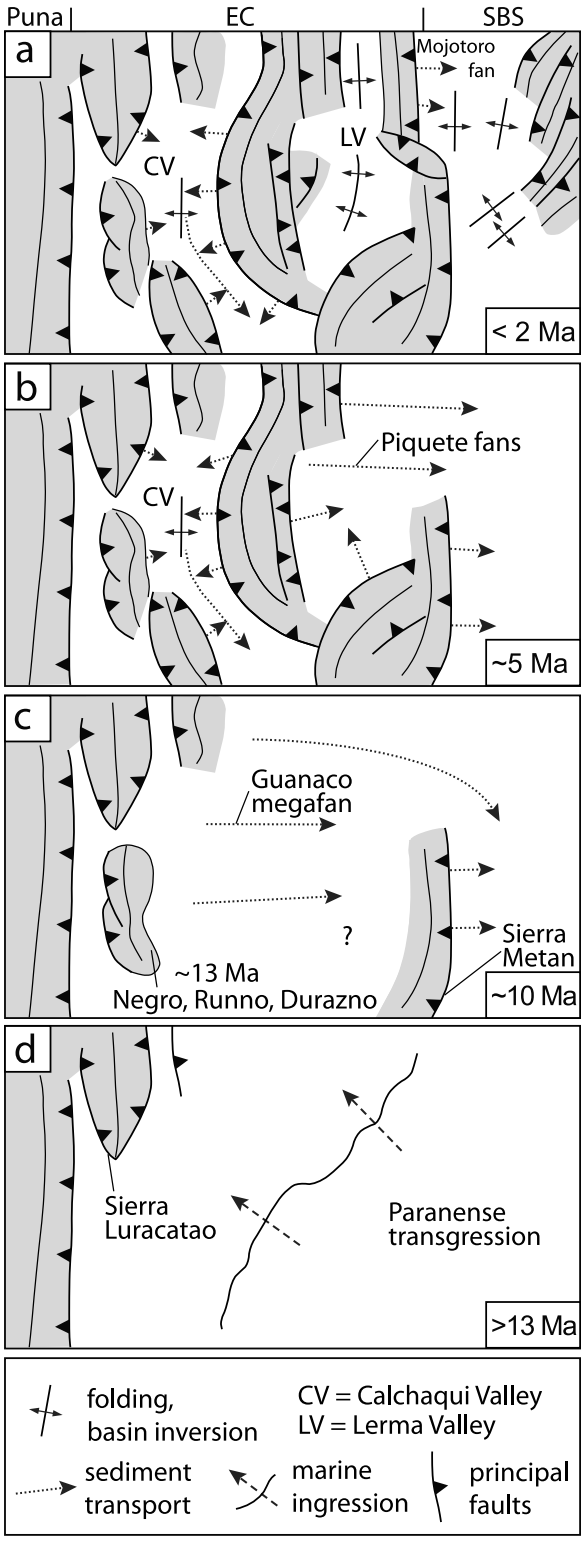

Figure 15. (a–d) Schematic overview of the Neogene fragmentation history of the Salta foreland, corresponding to the geographic extent of Figure 2.

Mio-Pliocene Santa María Group was deformed between 3.4 and 2.5 Ma [*Strecker et al.*, 1989; *Bossi et al.*, 2001].

[57] The latest stage of foreland fragmentation in the SBS and EC began during the Quaternary and is still locally ongoing (Figure 15a). For example, the Vaqueros/San Lorenzo anticlines (Figure 10) and the Lomas de Olmedo anticline in the far northeastern sector of the SBS [*Ramos et al.*, 2006] have experienced neotectonic deformation. Also pertaining to this episode, without evidence for Holocene deformation, are the uplift of the Sierra de Mojotoro and the accompanying intrabasin inversion of the Lerma Valley (eastern EC) and the SBS. For example, syndeformational to postdeformational deposits of the La Troja Formation have a strong compositional affinity to local sediment sources such as the central EC ranges or the ranges that separate the EC from the SBS (see section 4.2.3). Because uplift of the central SBS, including the Gonzalez, Lumbrera, San Antonio and Gallo ranges (Figure 2b), was structurally related to the deformation within the adjacent basins, where the Piquete Formation was being folded [e.g., *Kley and Monaldi*, 2002], we suggest that these range-bounding faults also became active during the Quaternary (Figure 15a). In addition, the unconformable alluvial fan deposits in the Mojotoro range piedmont (Figure 11) record the unroofing of that range during the Quaternary. Angular unconformities and growth strata separating the Piquete and La Troja formations have also been noted by *Salfity et al.* [2004] and *Carrera and Muñoz* [2008], leading them to propose a Quaternary deformation phase. Deformed basin fills and strath terraces in the Quebrada del Toro of the central EC [*Hilley and Strecker*, 2005; *Marrett and Strecker*, 2000], the Santa María Basin [*Strecker et al.*, 1989] and other adjacent areas [*Ramos et al.*, 2006; *Carrera and Muñoz*, 2008] further attest to Quaternary tectonic activity. Thus, Quaternary deformation is partitioned across the entire width of the Salta foreland.

[58] Although the ranges of the central SBS reduce the fluvial connectivity between the SBS and the open, undeformed Chaco foreland, protracted internal drainage conditions related to tectonically controlled hydrologic isolation, such as in the western EC and the Sierras Pampeanas [e.g., *Mortimer et al.*, 2007; *Strecker et al.*, 2007a], were apparently not established. The Lerma Valley, however, experienced extensive transient deposition of lacustrine sediments, well above the current base level of the SBS and the Chaco foreland [*Malamud et al.*, 1996] at present-day elevations of 1100 m, 800 m and 300 m, respectively.

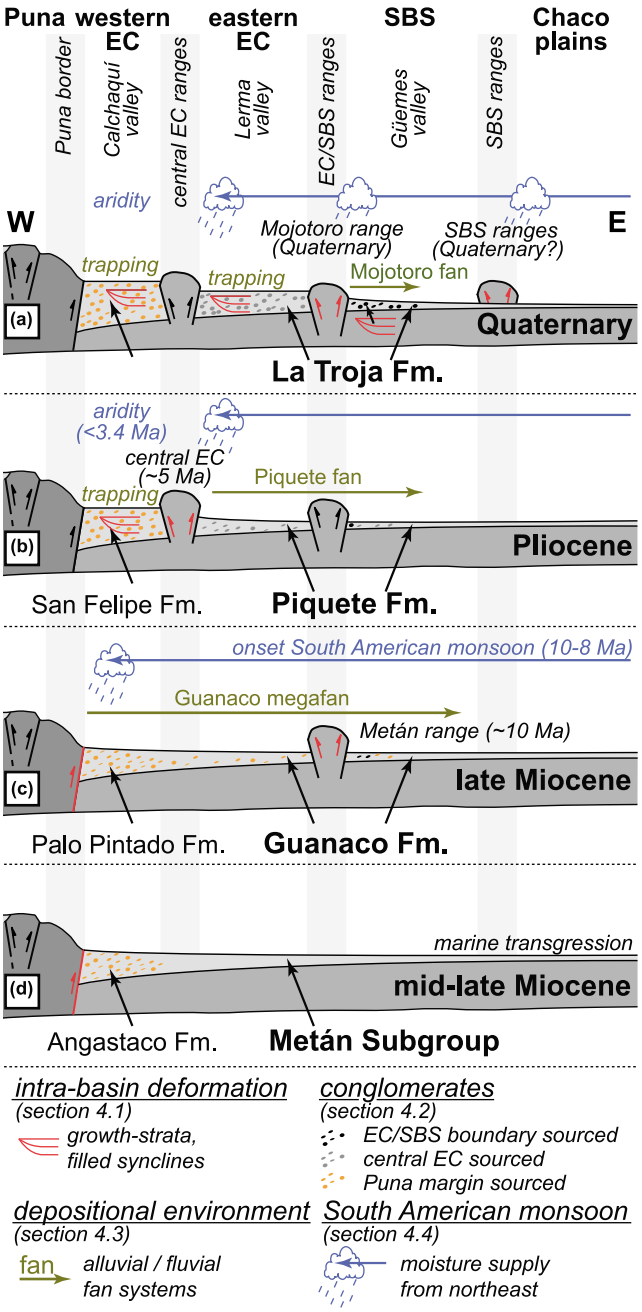

5.2. Tectonics, Climate and Sedimentation

[59] Given the subtropical latitude (~25°S) of the Salta foreland a perennial dry climate associated with descending air of the Hadley cell may be expected. Today, however, seasonal winds (i.e., the South American Monsoon System)

Figure 16. (a–d) Schematic overview synthesizing the relationship between tectonic forcing, hinterland aridification, and sediment dynamics during the Miocene to Quaternary. This ~200 km wide section corresponds roughly with swath 1 in Figures 13 and 14. Importantly, the thickness of the stratigraphic units is not to scale but rather serves to illustrate how trapping of sediment in the intermontane basins raises basin elevation, which promotes aridification (see section 4.4). The change from arid to more humid conditions at 10 to 8 Ma [e.g., *Starck and Anzótegui*, 2001; *Kleinert and Strecker*, 2001] has been related to the onset of the South American monsoon [*Strecker et al.*, 2007a, 2007b; *Mulch et al.*, 2010]. Semiarid conditions in the western EC after 3.4 Ma were described by *Coutand et al.* [2006]. The mid-Miocene marine transgression was described by *Ramos and Alonso* [1995] and *Hernández et al.* [2005].

import tropical moisture to the region during the austral summer [e.g., *Garreaud et al.*, 2003; *Vera et al.*, 2006a; *Seluchi et al.*, 2003; *Insel et al.*, 2009]. This highly seasonal climate pattern is thought to have persisted in the southern central Andes since 10–8 Ma [*Strecker et al.*, 2007a, 2007b; *Mulch et al.*, 2010] (Figure 16), probably related to uplift of the Andes [*Strecker et al.*, 2007a; *Ehlers and Poulsen*, 2009; *Insel et al.*, 2009; *Poulsen et al.*, 2010]. Below, we specifically consider the evolution of the local effects on climate patterns that caused the establishment of the present-day basin-to-basin gradients in moisture supply, rather than regional climate trends/shifts. Along these lines, we caution (1) that secular changes affecting subtropical (i.e., regional) climatic conditions since the establishment of the South American Monsoon are unresolved by our treatment and (2) that proxy-based paleoclimate reconstructions from distant locations [e.g., *Mulch et al.*, 2010] may not fully capture the history of external moisture supply to the Salta foreland.

[60] The two mechanisms for hinterland aridification that we identified in the Salta foreland (section 4.4) have important implications for sediment dynamics: reduced moisture reaching the intermontane basins lowers the efficiency of fluvial erosion processes where rivers traverse the bedrock of the uplifting ranges [e.g., *Roe et al.*, 2002; *Sobel et al.*, 2003; *Hilley and Strecker*, 2005] such that sediment storage within the orogen is favored over fluvial connectivity. We find that this dynamic may also apply to basins that are not separated by ranges exposing bedrock (i.e., Calchaquí and Santa Maria valleys). Sediment trapping in the hinterland raises the mean basin elevations and leads to further hinterland aridification. This clearly creates a positive feedback between aridification, severed drainage, and sediment storage. In this interrelated tectonic and climatic context, the stratigraphic record of the broken foreland as a whole and the spatiotemporal distribution of provenance signals in particular, may be reconciled.

[61] First, with the onset of the South American Low Level Jet as an integral part of the South American Monsoon [e.g., *Garreaud*, 1999; *Vera et al.*, 2006a, 2006b] between 10 and 8 Ma [*Strecker et al.*, 2007a, 2007b; *Mulch et al.*, 2010], seasonal moisture supply to the eastern flank of the Puna Plateau was largely unrestricted [e.g., *Starck and Anzótegui*, 2001; *Kleinert and Strecker*, 2001; *Alonso et al.*, 2006; *Coutand et al.*, 2006; *Strecker et al.*, 2007a; *Vezzoli et al.*, 2009] (Figure 16c). In southernmost Bolivia this coupling is expressed in increased sedimentation rates and the formation of fluvial megafans [*Horton and DeCelles*, 2001; *Leier et al.*, 2005; *Uba et al.*, 2005, 2007, 2009]. We infer that these changing climatic conditions also produced the Guanaco Formation megafan in the Salta foreland, which preserves the Puna border provenance signature across a depozone covering distances in excess of 100 km (Figure 16c). The isolated uplift of the Metán Range in the foreland provided an important local sediment source. However, (1) it did not constitute a laterally continuous orographic barrier, and thus could not prevent moisture from reaching the Puna border, and (2) it did not significantly restrict sediment export from the hinterland (Figure 16c).

[62] Second, at about 5 Ma, uplift of the central EC ranges intercepted sediment export from the western EC (Calchaquí Valley) promoting local sediment storage [e.g., *Kleinert and Strecker*, 2001; *Strecker et al.*, 2007a]. Consequently, throughout the eastern EC and the SBS the Puna border provenance signal was replaced with that of the central EC, suggesting that sediments derived from the Puna border were trapped in the hinterland rather than exported to the foreland (Figure 16b). Orographic precipitation along the central EC ranges caused sediment transport and deposition of the Piquete Formation alluvial fans, which were smaller than the Guanaco megafan but still extended from the central EC ranges into the SBS (>60 km; Figure 16b). Between 3.4 and 2.4 Ma continued uplift of the central EC ranges caused an effective orographic barrier with above-threshold relief, shielding the Calchaquí Valley from easterly moisture supply and thus giving rise to the modern arid conditions in the western EC [e.g., *Coutand et al.*, 2006], which reduced fluvial transport capacity and thus further promoted sediment trapping and aridity in the Calchaquí Valley.

[63] Third, Quaternary deformation has topographically isolated the Lerma Valley but has not yet resulted in an efficient orographic barrier capable of intercepting incoming easterly moisture-bearing winds (Figure 16a). Nevertheless, sediments shed from the central EC into the Lerma Valley are stored in kilometer-scale alluvial fans and synclines related to basin inversion. This Quaternary sediment storage in the eastern EC contributes a significant fraction to the ~300 m elevation difference between the Lerma Valley and the SBS (Figures 2b and 14a). We suggest that the modern conditions of the Lerma Valley (eastern EC) are analogous to the Calchaquí Valley (western EC) after ~5 Ma and before 3.4 to 2.4 Ma; in both cases topographic isolation caused intermontane sediment trapping rather than export, and incomplete orographic shielding allowed for moisture to penetrate into the hinterland.

[64] With respect to the dynamics of the adjacent Altiplano-Puna Plateau it is interesting to note that, with the late Miocene to Pliocene onset of the modern plateau precipitation regime (i.e., critical relief conditions along the plateau margin), none of the basins created by foreland fragmentation have been permanently isolated from the drainage system, one proposed mode of lateral plateau growth [*Sobel et al.*, 2003; *Barnes and Ehlers*, 2009]. In this regard one might speculate that, instead of facilitating the expansion of the plateau, the progressive hinterland aridification and associated sediment infilling achieved by foreland fragmentation preserves the present Puna border by guarding it from headwater erosion.

6. Summary and Conclusion

[65] In this study we have presented new stratigraphic, structural and climate observations that elucidate the relationships between tectonic forcing, precipitation patterns, and sediment dynamics of the broken Salta foreland in the southern central Andes. These observations argue for a three-phase history of progressive foreland compartmentalization: (1) at ~10 Ma uplift was partitioned between the western EC and the EC/SBS boundary, (2) at ~5 Ma uplift of the central EC ranges topographically isolated the western EC intermontane basin, and (3) since ~2 Ma diachronous deforma-

tion was partitioned across the entire foreland and has topographically isolated the eastern EC intermontane basin. The Quaternary deformation phase is ongoing. This first-order description of the timing and location of deformation provides hitherto unavailable constraints on the evolution of the Salta foreland domain.

[66] We document evidence for progressive storage of sediment in the hinterland intermontane basins, which appears to be aggravated by both tectonic ponding of the drainage system and orographically induced hinterland aridity (see Figure 16). Importantly, if sediments are trapped within rather than being exported from the orogen, they contribute to surface uplift in the basins and increase the topographic load. Herein, we identify basin elevation as one controlling factor of hinterland aridification, which suggests that intermontane sediment storage feeds back on basin-to-basin precipitation gradients. Furthermore, sediment trapping may also feed back on deformation because topographic loading raises lithostatic stress and causes deformation to propagate into the foreland. Overall, this study adds detail to the existing model of climate/tectonics interactions by providing specific examples of basin-scale and intrabasin sediment trapping even in the absence of internal drainage conditions.

[67] **Acknowledgments.** We thank Fernado Hongn, Nadine McQuarrie, and Victor A. Ramos for helpful discussions. Jason B. Barnes and an anonymous reviewer took the time to provide very detailed and insightful comments that led to a substantially improved manuscript. Strecker, Bookhagen, Alonso, and Pingel acknowledge funding by the DFG-Leibniz Center for Earth Surface Process and Climate Studies (grant STR 373/19-19). Schmitt acknowledges the use of the ion microprobe facility at UCLA, which is partly supported by a grant from the Instrumentation and Facilities Program, Division of Earth Sciences, National Science Foundation. The seismic data sets and borehole information from the Coronel Moldes area were kindly provided by YPF Repsol, S. A., Buenos Aires. Birgit Fabian helped preparing the figures.

References

Allmendinger, R. W., V. A. Ramos, T. E. Jordan, M. Palma, and B. L. Isacks (1983), Paleogeography and Andean structural geometry, northwest Argentina, *Tectonics*, *2*(1), 1–16, doi:10.1029/TC002i001p00001.

Allmendinger, R. W., T. E. Jordan, S. M. Kay, and B. L. Isacks (1997), The evolution of the Altiplano-Puna plateau of the central Andes, *Annu. Rev. Earth Planet. Sci.*, *25*, 139–174, doi:10.1146/annurev.earth.25.1.139.

Alonso, R. N., T. E. Jordan, K. T. Tabbutt, and D. S. Vandervoort (1991), Giant evaporite belts of the Neogene central Andes, *Geology*, *19*(4), 401–404, doi:10.1130/0091-7613(1991)019<0401:GEBOTN>2.3.CO;2.

Alonso, R. N., B. Carrapa, I. Coutand, M. Haschke, and G. E. Hilley (2006), Tectonics, climate and landscape evolution of the southern central Andes: The Argentine Puna Plateau and adjacent regions between 22 and 28°S lat, in *The Andes: Active Subduction Orogeny*, edited by O. Oncken et al., pp. 265–283, Springer, Berlin.

Baldis, B. A. J., A. Gorroño, J. V. Ploszkiewitz, and R. M. Sarudiansky (1976), Geotéctonica de la Cordillera Oriental, Sierras Subandinas y comarcas adjacentes, paper presented at VI Congreso Geológico Argentino, Asoc. Geol. Argent., Bahía Blanca, Argentina.

Barnes, J. B., and T. A. Ehlers (2009), End member models for Andean Plateau uplift, *Earth Sci. Rev.*, *97*(1–4), 105–132, doi:10.1016/j.earscirev.2009.08.003.

Bianucci, H. A., and J. F. Homovec (1982), Tectogénesis de un sector de la cuenca del Subgrupo Pirgua, noroeste Argentina, paper presented at V Congreso Latinoamericano Geológico, Asoc. Geol. Argent., Buenos Aires.

Blair, T. C., and J. G. McPherson (1994), Alluvial fans and their natural distinction from rivers based on morphology, hydraulic processes, sedimentary processes, and facies assemblages, *J. Sediment. Res.*, *A64*, 450–489.

Bookhagen, B., and D. W. Burbank (2010), Toward a complete Himalayan hydrological budget: Spatiotemporal distribution of snowmelt and rainfall and their impact on river discharge, *J. Geophys. Res.*, *115*, F03019, doi:10.1029/2009JF001426.

Bookhagen, B., and M. R. Strecker (2008), Orographic barriers, high-resolution TRMM rainfall, and relief variations along the eastern Andes, *Geophys. Res. Lett.*, *35*, L06403, doi:10.1029/2007GL032011.

Bookhagen, B., K. Haselton, and M. H. Trauth (2001), Hydrological modelling of a Pleistocene landslide-dammed lake in the Santa Maria Basin, NW Argentina, *Palaeogeogr. Palaeoclimatol. Palaeoecol.*, *169*(1–2), 113–127, doi:10.1016/S0031-0182(01)00221-8.

Bosio, P. P., J. Powell, C. del Papa, and F. Hongn (2009), Middle Eocene deformation-sedimentation in the Luracatao Valley: Tracking the beginning of the foreland basin of northwestern Argentina, *J. South Am. Earth Sci.*, *28*(2), 142–154, doi:10.1016/j.jsames.2009.06.002.

Bossi, G. E., S. M. Georgieff, I. J. C. Gavriloff, L. M. Ibañez, and C. M. Muruaga (2001), Cenozoic evolution of the intramontane Santa María basin, Pampean Ranges, northwestern Argentina, *J. South Am. Earth Sci.*, *14*(7), 725–734, doi:10.1016/S0895-9811(01)00058-X.

Bourdon, B., G. Wörner, and A. Zindler (2000), U-series evidence for crustal involvement and magma residence times in the petrogenesis of Parinacota volcano, Chile, *Contrib. Mineral. Petrol.*, *139*, 458–469, doi:10.1007/s004100000150.

Bywater-Reyes, S., B. Carrapa, M. Clementz, and L. Schoenbohm (2010), Effect of late Cenozoic aridification on sedimentation in the Eastern Cordillera of northwest Argentina (Angastaco basin), *Geology*, *38*(3), 235–238, doi:10.1130/G30532.1.

Carrapa, B., J. Hauer, L. Schoenbohm, M. R. Strecker, A. K. Schmitt, A. Villanueva, and J. Sosa Gomez (2008), Dynamics of deformation and sedimentation in the northern Sierras Pampeanas: An integrated study of the Neogene Fiambalá basin, NW Argentina, *Geol. Soc. Am. Bull.*, *120*(11–12), 1518–1543, doi:10.1130/B26111.1.

Carrera, N., and J. A. Muñoz (2008), Thrusting evolution in the southern Cordillera Oriental (northern Argentine Andes): Constraints from growth strata, *Tectonophysics*, *459*, 107–122, doi:10.1016/j.tecto.2007.11.068.

Carrera, N., J. A. Muñoz, F. Sábat, R. Mon, and E. Roca (2006), The role of inversion tectonics in the structure of the Cordillera Oriental (NW Argentinean Andes), *J. Struct. Geol.*, *28*(11), 1921–1932, doi:10.1016/j.jsg.2006.07.006.

Coutand, I., P. R. Cobbold, M. de Urreiztieta, P. Gautier, A. Chauvin, D. Gapais, E. A. Rossello, and O. López-Gamundí (2001), Style and history of Andean deformation, Puna plateau, northwestern Argentina, *Tectonics*, *20*(2), 210–234, doi:10.1029/2000TC900031.

Coutand, I., B. Carrapa, A. Deeken, A. K. Schmitt, E. R. Sobel, and M. R. Strecker (2006), Propagation of orographic barriers along an active range front: Insights from sandstone petrography and detrital apatite fission-track thermochronology in the intramontane Angastaco basin, NW Argentina, *Basin Res.*, *18*(1), 1–26, doi:10.1111/j.1365-2117.2006.00283.x.

Cristallini, E., A. H. Cominguez, and V. A. Ramos (1997), Deep structure of the Metan-Guachipas region: Tectonic inversion in northwestern Argentina, *J. South Am. Earth Sci.*, *10*(5–6), 403–421, doi:10.1016/S0895-9811(97)00026-6.

Davis, S. J., A. Mulch, A. R. Carroll, T. W. Horton, and C. P. Chamberlain (2009), Paleogene landscape evolution of the central North American Cordillera: Developing topography and hydrology in the Laramide foreland, *Geol. Soc. Am. Bull.*, *121*(1–2), 100–116.

DeCelles, P. G., and K. A. Giles (1996), Foreland basin systems, *Basin Res.*, *8*(2), 105–123, doi:10.1046/j.1365-2117.1996.01491.x.

Deeken, A., E. R. Sobel, I. Coutand, M. Haschke, U. Riller, and M. R. Strecker (2006), Development of the southern Eastern Cordillera, NW Argentina, constrained by apatite fission track thermochronology: From early Cretaceous extension to middle Miocene shortening, *Tectonics*, *25*, TC6003, doi:10.1029/2005TC001894.

Díaz, J., and D. Malizzia (1984), Estudio geológico y sedimentológico del Terciario Superior del Valle Calchaquí (Dpto. San Carlos; Salta), *Bol. Sedimentol.*, *2*, 8–28.

Durand, F. R., and J. N. Rossi (1999), Metamorfismo del sector NE de las Cumbres Calchaquíes, sierra de San Javier y serranías de noreste de Tucumán, in *Geología del Noroeste Argentino*, edited by G. Bonorino, R. Omarini, and J. Viramonte, pp. 52–57, Univ. Nac. de Salta, Salta, Argentina.

Ehlers, T. A., and C. J. Poulsen (2009), Influence of Andean uplift on climate and paleoaltimetry estimates, *Earth Planet. Sci. Lett.*, *281*(3–4), 238–248, doi:10.1016/j.epsl.2009.02.026.

Ernst, W. G. (2010), Young convergent-margin orogens, climate, and crustal thickness—A Late Cretaceous–Paleogene Nevadaplano in the American Southwest?, *Lithosphere*, *2*(2), 67–75, doi:10.1130/L84.1.

Galewsky, J. (2009), Rain shadow development during the growth of mountain ranges: An atmospheric dynamics perspective, *J. Geophys. Res.*, *114*, F01018, doi:10.1029/2008JF001085.

Galli, C. I., R. M. Hernández, and J. H. Reynolds (1996), Análisis paleoambiental y ubicación geocronológica del Subgrupo Metán (Grupo Orán, Neógeno) en el Río Piedras, departmento Metán: Salta, Argentina, *Bol. Inf. Petrol. Tercera Epoca*, *12*, 99–107.

Garreaud, R. D. (1999), Multiscale analysis of the summertime precipitation over the central Andes, *Mon. Weather Rev.*, *127*(5), 901–921, doi:10.1175/1520-0493(1999)127<0901:MAOTSP>2.0.CO;2.

Garreaud, R., M. Vuille, and A. C. Clement (2003), The climate of the Altiplano: Observed current conditions and mechanisms of past changes, *Palaeogeogr. Palaeoclimatol. Palaeoecol.*, *194*(1–3), 5–22, doi:10.1016/S0031-0182(03)00269-4.

Gebhard, J. A., A. R. Guidice, and J. O. Gascon (1974), Geología de la comarca entre el Río Juramento y Arroyo las Tortugas, provincias de Salta y Jujuy, *Rev. Asoc. Geol. Argent.*, *29*, 359–375.

Gonzalez Villa, R. E. (2002), El subgrupo Jujuy (Neogeno) entre los 24°–26°LS y 64°–66°LO, tramo cento austral de la cadena subandina Argentina, provincias de Salta y Jujuy, Ph.D. thesis, Univ. Nac. de Salta, Salta, Argentina.

Grier, M. E. (1990), The influence of the Cretaceous Salta rift basin on the development of Andean structural geometries, NW Argentine Andes, Ph.D. thesis, Cornell Univ., Ithaca, N. Y.

Grier, M. E., and R. D. Dallmeyer (1990), Age of the Payogastilla Group: Implications for foreland basin development, NW Argentina, *J. South Am. Earth Sci.*, *3*(4), 269–278, doi:10.1016/0895-9811(90)90008-O.

Grier, M. E., J. A. Salfity, and R. W. Allmendinger (1991), Andean reactivation of the Cretaceous Salta rift, northwestern Argentina, *J. South Am. Earth Sci.*, *4*(4), 351–372, doi:10.1016/0895-9811(91)90007-8.

Grove, M., C. E. Jacobson, A. P. Barth, and A. Vucic (2003), Temporal and spatial trends of Late Cretaceous–Early Tertiary underplating of Pelona and related schist beneath southern California and southwestern Arizona, *Spec. Pap. Geol. Soc. Am.*, *374*, 381–406.

Hain, M. P. (2008), *Neogene Foreland Evolution of the Southern Central Andes and Its Relationship to Ancient Strain History and Varying Climates*, 94 pp., Univ. Potsdam, Potsdam, Germany.

Hain, M. P., and M. R. Strecker (2008), Control of Cretaceous extensional and inherited basement structures on position and style of Andean shortening—Valle de Lerma, Salta, NW Argentina, paper presented at XVII Congreso Geológico Argentino, Asoc. Geol. Argent., San Salvador de Jujuy, Argentina.

Haines, P. W., M. Hand, and M. Sandiford (2001), Palaeozoic synorogenic sedimentation in central and northern Australia: A review of distribution and timing with implications for the evolution of intracontinental orogens, *Aust. J. Earth Sci.*, *48*(6), 911–928, doi:10.1046/j.1440-0952.2001.00909.x.

Hernández, R. M., T. E. Jordan, A. Dalenz Farjat, L. Echavarría, B. D. Idleman, and J. H. Reynolds (2005), Age, distribution, tectonics, and eustatic controls of the Paranense and Caribbean marine transgressions in southern Bolivia and Argentina, *J. South Am. Earth Sci.*, *19*(4), 495–512, doi:10.1016/j.jsames.2005.06.007.

Hilley, G. E., and M. R. Strecker (2005), Processes of oscillatory basin filling and excavation in a tectonically active orogen: Quebrada del Toro Basin, NW Argentina, *Geol. Soc. Am. Bull.*, *117*(7–8), 887–901, doi:10.1130/B25602.1.

Holton, J. R. (1992), *An Introduction to Dynamic Meteorology*, 497 pp., Academic, San Diego, Calif.

Hongn, F. D., and U. Riller (2007), Tectonic evolution of the western margin of Gondwana inferred from syntectonic emplacement of Paleozoic granitoid plutons in northwest Argentina, *J. Geol.*, *115*(2), 163–180, doi:10.1086/510644.

Hongn, F., C. del Papa, J. Powell, I. Petrinovic, R. Mon, and V. Deraco (2007), Middle Eocene deformation and sedimentation in the Puna–Eastern Cordillera transition (23°–26°S): Control by preexisting heterogeneities on the pattern of initial Andean shortening, *Geology*, *35*(3), 271–274, doi:10.1130/G23189A.1.

Hongn, F., R. Mon, I. Petrinovic, C. Del Papa, and J. Powell (2008), Inversión tectonica en el noroeste Argentino: Influencia de las heterogeneidades del basamento, paper presented at XVII Congreso Geológico Argentino, Asoc. Geol. Argent., San Salvador de Jujuy, Argentina.

Hongn, F., R. Mon, I. Petrinovic, C. Del Papa, and J. Powell (2010), Inversión y reactivación tectónicas Cretácico-Cenozoicas en el noroeste Argentino: Influencia de las heterogeneidades del basamento Neoproterozoico-Paleozoico inferior, *Asoc. Geol. Argent. Rev.*, *66*, 38–53.

Horton, B. K., and P. G. DeCelles (2001), Modern and ancient fluvial megafans in the foreland basin system of the central Andes, southern Bolivia: Implications for drainage network evolution in fold-thrust belts, *Basin Res.*, *13*(1), 43–63, doi:10.1046/j.1365-2117.2001.00137.x.

Howard, K. A., and B. E. John (1997), Fault-related folding during extension: Plunging basement-cored folds in the basin and range, *Geology*, *25*(3), 223–226, doi:10.1130/0091-7613(1997)025<0223:FRFDEP>2.3.CO;2.

Insel, N., C. J. Poulsen, and T. A. Ehlers (2009), Influence of the Andes Mountains on South American moisture transport, convection, and precipitation, *Clim. Dyn.*, *35*, 1477–1492, doi:10.1007/s00382-009-0637-1.

Janecke, S. U., C. J. Vandenburg, and J. J. Blankenau (1998), Geometry, mechanisms and significance of extensional folds from examples in the Rocky Mountain Basin and Range province, U.S.A., *J. Struct. Geol.*, *20*(7), 841–856, doi:10.1016/S0191-8141(98)00016-9.

Ježek, P., A. P. Willner, F. G. Aceñolaza, and H. Miller (1985), The Puncoviscana trough—A large basin of late Precambrian to early Cambrian age on the Pacific edge of the Brazilian shield, *Geol. Rundsch.*, *74*, 573–584, doi:10.1007/BF01821213.

Jordan, T. E., and R. W. Allmendinger (1986), The Sierras Pampeanas of Argentina—A modern analog of Rocky-Mountain foreland deformation, *Am. J. Sci.*, *286*(10), 737–764, doi:10.2475/ajs.286.10.737.

Jordan, T. E., and R. N. Alonso (1987), Cenozoic stratigraphy and basin tectonics of the Andes Mountains, 20°–28° south latitude, *AAPG Bull.*, *71*, 49–64.

Kleinert, K., and M. R. Strecker (2001), Climate change in response to orographic barrier uplift: Paleosol and stable isotope evidence from the late Neogene Santa Maria basin, northwestern Argentina, *Geol. Soc. Am. Bull.*, *113*(6), 728–742, doi:10.1130/0016-7606(2001)113<0728:CCIRTO>2.0.CO;2.

Kley, J., and C. R. Monaldi (2002), Tectonic inversion in the Santa Barbara System of the central Andean foreland thrust belt, northwestern Argentina, *Tectonics*, *21*(6), 1061, doi:10.1029/2002TC902003.

Kley, J., E. A. Rossello, C. R. Monaldi, and B. Habighorst (2005), Seismic and field evidence for selective inversion of Cretaceous normal faults, Salta rift, northwest Argentina, *Tectonophysics*, *399*, 155–172, doi:10.1016/j.tecto.2004.12.020.

Leier, A., P. G. DeCelles, and J. D. Pelletier (2005), Mountains, monsoons, and megafans, *Geology*, *33*(4), 289–292, doi:10.1130/G21228.1.

Malamud, B. D., T. E. Jordan, R. N. Alonso, R. E. Gallardo, R. E. González, and S. A. Kelley (1996), Pleistocene Lake Lerma, Salta Province, NW Argentina, paper presented at XIII Congreso Geológico Argentino, Asoc. Geol. Argent., Buenos Aires.

Marquillas, R. A., and J. A. Salfity (1988), Tectonic framework and correlations of the Cretaceous-Eocene Salta Group, Argentina, in *The Southern Central Andes*, edited by H. Bahlburg, C. Breitkreuz, and P. Giese, pp. 119–136, doi:10.1007/BFb0045178, Springer, Berlin.

Marrett, R., and M. R. Strecker (2000), Response of intracontinental deformation in the central Andes to late Cenozoic reorganization of South American Plate motions, *Tectonics*, *19*(3), 452–467, doi:10.1029/1999TC001102.

Marshak, S., K. Karlstrom, and J. M. Timmons (2000), Inversion of Proterozoic extensional faults: An explanation for the pattern of Laramide and Ancestral Rockies intracratonic deformation, United States, *Geology*, *28*(8), 735–738, doi:10.1130/0091-7613(2000)28<735:IOPEFA>2.0.CO;2.

Marshall, L. G., R. Hoffstetter, and R. Pascual (1983), *Mammals and Stratigraphy: Geochronology of the Continental Mammal-Bearing Tertiary of South America*, vol. 93, *Palaeovertebrata*, Lab. de Paléontol. des Vertébrés de l'École Pratique de Hautes Études, Montpellier, France.

Mon, R., and F. Hongn (1991), The structure of the Precambrian and Lower Paleozoic basement of the central Andes between 22° and 32°S lat, *Geol. Rundsch.*, *80*, 745–758, doi:10.1007/BF01803699.

Mon, R., and J. A. Salfity (1995), Tectonic evolution of the Andes of northern Argentina, in *Petroleum Basins of South America*, edited by A. J. Tankard, R. Suárez Soruco, and H. J. Welsink, pp. 269–283, Am. Assoc. Petrol. Geol., Tulsa, Okla.

Monaldi, C. R., R. E. Gonzalez, and J. A. Salfity (1996), Thrust fronts in the Lerma Valley (Salta, Argentina) during the Piquete Formation deposition (Pliocene-Pleistocene), paper presented at 3rd International Symposium on Andean Geodynamics, St. Malo, France.

Mora, A., M. Parra, M. R. Strecker, A. Kammer, C. Dimaté, and F. Rodríguez (2006), Cenozoic contractional reactivation of Mesozoic extensional structures in the Eastern Cordillera of Colombia, *Tectonics*, *25*, TC2010, doi:10.1029/2005TC001854.

Mora, A., T. Gaona, J. Kley, D. Montoya, M. Parra, L. I. Quiroz, G. Reyes, and M. R. Strecker (2009), The role of inherited extensional fault segmentation and linkage in contractional orogenesis: A reconstruction of Lower Cretaceous inverted rift basins in the Eastern Cordillera of Colombia, *Basin Res.*, *21*(1), 111–137, doi:10.1111/j.1365-2117.2008.00367.x.

Mortimer, E., B. Carrapa, I. Coutand, L. Schoenbohm, E. R. Sobel, J. S. Gomez, and M. R. Strecker (2007), Fragmentation of a foreland basin in response to out-of-sequence basement uplifts and structural reactivation: El Cajón–Campo del Arenal basin, NW Argentina, *Geol. Soc. Am. Bull.*, *119*(5–6), 637–653, doi:10.1130/B25884.1.

Mulch, A., C. E. Uba, M. R. Strecker, R. Schoenberg, and C. P. Chamberlain (2010), Late Miocene climate variability and surface elevation in the central Andes, *Earth Planet. Sci. Lett.*, *290*(1–2), 173–182, doi:10.1016/j.epsl.2009.12.019.

Paces, J. B., and J. D. Miller Jr. (1993), Precise U-Pb ages of Duluth complex and related mafic intrusions, northeastern Minnesota: Geochronological insights to physical, petrogenetic, paleomagnetic, and tectonomagmatic processes associated with the 1.1 Ga midcontinent rift system, *J. Geophys. Res.*, *98*(B8), 13,997–14,013, doi:10.1029/93JB01159.

Parra, M., A. Mora, E. R. Sobel, M. R. Strecker, and R. González (2009a), Episodic orogenic front migration in the northern Andes: Constraints from low-temperature thermochronology in the Eastern Cordillera, Colombia, *Tectonics*, *28*, TC4004, doi:10.1029/2008TC002423.

Parra, M., A. Mora, C. Jaramillo, M. R. Strecker, E. R. Sobel, L. Quiroz, M. Rueda, and V. Torres (2009b), Orogenic wedge advance in the northern Andes: Evidence from the Oligocene-Miocene sedimentary record of the Medina Basin, Eastern Cordillera, Colombia, *Geol. Soc. Am. Bull.*, *121*(5–6), 780–800, doi:10.1130/B26257.1.

Poulsen, C. J., T. A. Ehlers, and N. Insel (2010), Onset of convective rainfall during gradual Late Miocene rise of the central Andes, *Science*, *328*(5977), 490–493, doi:10.1126/science.1185078.

Ramos, V. A. (2008), The basement of the central Andes: The Arequipa and related terranes, *Annu. Rev. Earth Planet. Sci.*, *36*, 289–324, doi:10.1146/annurev.earth.36.031207.124304.

Ramos, V. A., and R. N. Alonso (1995), El mar paranense en la provincia de Jujuy, *Rev. Inst. Geol. Min.*, *10*, 73–82.

Ramos, V. A., R. N. Alonso, and M. R. Strecker (2006), Estructura y Neotectónica de la Lomas de Olmedo, Zona de transición entre los sistemas Subandino y de Santa Bárbara Provincia de Salta, *Asoc. Geol. Argent. Rev.*, *4*, 579–588.

Reid, M. R., C. D. Coath, T. M. Harrison, and K. D. McKeegan (1997), Ion microprobe dating of young zircons reveals prolonged residence times for the youngest rhyolites associated with Long Valley caldera, *Earth Planet. Sci. Lett.*, *150*(1–2), 27–39, doi:10.1016/S0012-821X(97)00077-0.

Reynolds, J. H., B. D. Idleman, R. M. Hernández, and C. W. Naeser (1994), Preliminary chronostratigraphic constraints on Neogene tectonic activity in the Eastern Codillera and Santa Barbara System, Salta Province, NW Argentina, *Geol. Soc. Am. Abstr. Programs*, *26*, A503.

Reynolds, J. H., C. I. Galli, R. M. Hernández, B. D. Idleman, J. M. Kotila, R. V. Hillard, and C. W. Naeser (2000), Middle Miocene tectonic development of the transition zone, Salta Province, northwest Argentina: Magnetic stratigraphy from the Metan Subgroup, Sierra de Gonzalez, *Geol. Soc. Am. Bull.*, *112* (11), 1736–1751, doi:10.1130/0016-7606(2000)112<1736:MMTDOT>2.0.CO;2.

Richter, A. (2002), Provenance analysis of the San Felipe Formation (Pliocene) and Quaternary terrace gravels, Angastaco Basin, Calchaquí Valley, NW Argentina: SFB 267 deformation processes in the Andes, DFG progress report, Univ. Potsdam, Potsdam, Germany.

Roe, G. H. (2005), Orographic precipitation, *Annu. Rev. Earth Planet. Sci.*, *33*, 645–671, doi:10.1146/annurev.earth.33.092203.122541.

Roe, G. H., D. R. Montgomery, and B. Hallet (2002), Effects of orographic precipitation variations on the concavity of steady-state river profiles, *Geology*, *30*(2), 143–146.

Rolleri, E. O. (1976), Sistema de Santa Barbara: Una nueva provincia geológica Argentia, paper presented at VI Congreso Geológico Argentino, Asoc. Geol. Argent., Bahía Blanca, Argentina.

Ruíz Huídobro, O. J. (1968), Descripción geológica de la Hoja 7 e, Salta, provincias de Salta y Jujuy, *Bol. Dir. Nac. Geol. Min.*, *109*, 1–46.

Russo, A., and A. Serraiotto (1978), Contribución al conocimiento de la estratigrafía terciaria en el noroeste Argentino, paper presented at VII Congreso Geológico Argentino, Asoc. Geol. Argent., Neuquén, Argentina.

Salfity, J. A. (1982), Evolución paleogeográfica del Grupo Salta (Cretácico-Eogénico), Argentina, paper presented at V Congreso Latinoamericano de Geología, Asoc. Geol. Argent., Buenos Aires.

Salfity, J., R. Monaldi, R. Marquillas, and R. Gonzalez (1993), La inversión tectónica del Umbral de los Gallos en la cuenca del Grupo Salta durante la fase Incaica, paper presented at XII Congreso Geológico Argentino, Asoc. Geol. Argent., Mendoza, Argentina.

Salfity, J. A., C. R. Monaldi, F. Guidi, and R. J. Salas (1998), Mapa geológico de la provincia de Salta, Inst. de Geol. y Recursos Mineral., Buenos Aires.

Salfity, J. A., E. F. Gallardo, J. E. Sastre, and J. Esteban (2004), El lago cuaternario de Angastaco, Valle Calchaquí, Salta, *Asoc. Geol. Argent. Rev.*, *59*, 312–316.

Schmitt, A. K., D. F. Stockli, and B. P. Hausback (2006), Eruption and magma crystallization ages of Las Tres Vírgenes (Baja California) constrained by combined $^{230}Th/^{238}U$ and (U-Th)/He dating of zircon, *J. Volcanol. Geotherm. Res.*, *158*(3–4), 281–295, doi:10.1016/j.jvolgeores.2006.07.005.

Schmitt, A. K., D. F. Stockli, J. M. Lindsay, R. Robertson, O. M. Lovera, and R. Kislitsyn (2010), Episodic growth and homogenization of plutonic roots in arc volcanoes from combined U-Th and (U-Th)/He zircon dating, *Earth Planet. Sci. Lett.*, *295*(1–2), 91–103, doi:10.1016/j.epsl.2010.03.028.

Seluchi, M. E., A. C. Saulo, M. Nicolini, and P. Satyamurty (2003), The northwestern Argentinean low: A study of two typical events, *Mon. Weather Rev.*, *131*(10), 2361–2378, doi:10.1175/1520-0493(2003)131<2361:TNALAS>2.0.CO;2.

Sial, A. N., V. P. Ferreira, A. J. Toselli, F. G. Aceñolaza, M. M. Pimentel, M. A. Parada, and R. N. Alonso (2001), C and Sr isotopic evolution of carbonate sequences in NW Argentina: Implications for a probable Precambrian-Cambrian transition, *Carbonates Evaporites*, *16*(2), 141–152, doi:10.1007/BF03175832.

Sobel, E. R., and T. A. Dumitru (1997), Thrusting and exhumation around the margins of the western Tarim basin during the India-Asia collision, *J. Geophys. Res.*, *102*(B3), 5043–5063, doi:10.1029/96JB03267.

Sobel, E. R., and M. R. Strecker (2003), Uplift, exhumation and precipitation: Tectonic and climatic control of Late Cenozoic landscape evolution in the northern Sierras Pampeanas, Argentina, *Basin Res.*, *15*(4), 431–451, doi:10.1046/j.1365-2117.2003.00214.x.

Sobel, E. R., G. E. Hilley, and M. R. Strecker (2003), Formation of internally drained contractional basins by aridity-limited bedrock incision, *J. Geophys. Res.*, *108*(B7), 2344, doi:10.1029/2002JB001883.

Starck, D., and L. M. Anzótegui (2001), The late Miocene climatic change—Persistence of a climatic signal through the orogenic stratigraphic record in northwestern Argentina, *J. South Am. Earth Sci.*, *14*(7), 763–774, doi:10.1016/S0895-9811(01)00066-9.

Starck, D., and G. Vergani (1996), Desarrollo tectosedimentario del Cenozoico en el sur de la Provincia de Salta—Argentina, paper presented at XIII Congreso Geológico Argentino, Asoc. Geol. Argent., Buenos Aires.

Strecker, M. R., and R. Marrett (1999), Kinematic evolution of fault ramps and its role in development of landslides and lakes in the northwestern Argentine Andes, *Geology*, *27*(4), 307–310, doi:10.1130/0091-7613(1999)027<0307:KEOFRA>2.3.CO;2.

Strecker, M. R., P. Cerveny, A. L. Bloom, and D. Malizia (1989), Late Cenozoic tectonism and landscape development in the foreland of the Andes: Northern Sierras Pampeanas (26°–28°S), Argentina, *Tectonics*, *8*(3), 517–534, doi:10.1029/TC008i003p00517.

Strecker, M. R., R. N. Alonso, B. Bookhagen, B. Carrapa, G. E. Hilley, E. R. Sobel, and M. H. Trauth (2007a), Tectonics and climate of the southern central Andes, *Annu. Rev. Earth Planet. Sci.*, *35*, 747–787, doi:10.1146/annurev.earth.35.031306.140158.

Strecker, M. R., A. Mulch, C. Uba, A. Schmitt, and P. Chamberlain (2007b), Climate change in the southern central Andes at 8 Ma, *Geochim. Cosmochim. Acta*, *71*(15), A980.

Strecker, M. R., R. Alonso, B. Bookhagen, B. Carrapa, I. Coutand, M. P. Hain, G. E. Hilley, E. Mortimer, L. Schoenbohm, and E. R. Sobel (2009), Does the topographic distribution of the central Andean Puna Plateau result from climatic or geodynamic processes?, *Geology*, *37*(7), 643–646, doi:10.1130/G25545A.1.

Strecker, M. R., G. E. Hilley, B. Bookhagen, and E. R. Sobel (2011), Structural, geomorphic and depositional characteristics of contiguous and broken foreland basins: Examples from the eastern flanks of the central Andes in Bolivia and NW Argentina, in *Recent Advances in Tectonics of Sedimentary Basins*, edited by C. Busby and A. Azor, Blackwell, Boston, Mass.

Talling, P. J., T. F. Lawton, D. W. Burbank, and R. S. Hobbs (1995), Evolution of latest Cretaceous-Eocene nonmarine deposystems in the Axhandle piggyback basin of central Utah, *Geol. Soc. Am. Bull.*, *107*(3), 297–315, doi:10.1130/0016-7606(1995)107<0297:EOLCEN>2.3.CO;2.

Tapponnier, P., et al. (1990), Active thrusting and folding in the Qilian-Shan, and decoupling between upper crust and mantle in the northeastern Tibet, *Earth Planet. Sci. Lett.*, *97*(3–4), 382–403, doi:10.1016/0012-821X(90)90053-Z.

Turner, J. C. M. (1970), The Andes of northwestern Argentina, *Geol. Rundsch.*, *59*, 1028–1063, doi:10.1007/BF02042283.

Uba, C. E., C. Heubeck, and C. Hulka (2005), Facies analysis and basin architecture of the Neogene Subandean synorogenic wedge, southern Bolivia, *Sediment. Geol.*, *180*(3–4), 91–123.

Uba, C. E., M. R. Strecker, and A. K. Schmitt (2007), Increased sediment accumulation rates and climatic forcing in the central Andes during the late Miocene, *Geology*, *35*(11), 979–982, doi:10.1130/G224025A.1.

Uba, C. E., J. Kley, M. R. Strecker, and A. K. Schmitt (2009), Unsteady evolution of the Bolivian Subandean thrust belt: The role of enhanced erosion and clastic wedge progradation, *Earth Planet. Sci. Lett.*, *281*(3–4), 134–146, doi:10.1016/j.epsl.2009.02.010.

Vandervoort, D. S., T. E. Jordan, P. K. Zeitler, and R. N. Alonso (1995), Chronology of internal drainage development and uplift, southern Puna Plateau, Argentine central Andes, *Geology*, *23*(2), 145–148, doi:10.1130/0091-7613(1995)023<0145:COIDDA>2.3.CO;2.

Vera, C., et al. (2006a), Toward a unified view of the American Monsoon Systems, *J. Clim.*, *19*(20), 4977–5000, doi:10.1175/JCLI3896.1.

Vera, C., et al. (2006b), The South American low-level jet experiment, *Bull. Am. Meteorol. Soc.*, *87*(1), 63–77, doi:10.1175/BAMS-87-1-63.

Vergani, G., and D. Starck (1988), Geología del Sur de la Provincia de Salta—Parte I: Estratigrafía y evolución tectosedimentaria del Cenozoico entre el Valle de Lerma, report, Yacimientos Petrol. Fiscales, Buenos Aires.

Vergani, G., and D. Starck (1989a), Aspectos estructurales del Valle de Lerma al sur de la ciudad de Salta, *Bol. Inf. Petrol.*, *20*, 2–9.

Vergani, G., and D. Starck (1989b), Geología del Sur de la Provincia de Salta—Parte II: Estratigrafía y evolución tectosedimentaria del Cenozoico entre el Valle Calchaquí y Metán, report, Yacimientos Petrol. Fiscales, Buenos Aires.

Vezzoli, L., M. Matteini, N. Hauser, R. Omarini, R. Mazzuoli, and V. Acocella (2009), Non-explosive magma-water interaction in a continental setting: Miocene examples from the Eastern Cordillera (central Andes; NW Argentina), *Bull. Volcanol.*, *71*(5), 509–532, doi:10.1007/s00445-008-0239-5.

Viramonte, J. G., R. H. Omarini, V. Ara-Asaavedra, A. Aparicio, L. Garcia Cacho, and P. Parica (1984), Edad, genesis y mecanismos de erupción de las riolitas granatlferas de San Antonio de los Cobres, provincia de Salta, paper presented at IX Congreso Geológico Argentino, Asoc. Geol. Argent., San Carlos de Bariloche, Argentina.

Viramonte, J. G., J. H. Reynolds, C. Del Papa, and A. Disalvo (1994), The Corte Blanco garnetiferous tuff: A distinctive late Miocene marker bed in northwestern Argentina applied to magnetic polarity stratigraphy in the Río Yacones, Salta Province, *Earth Planet. Sci. Lett.*, *121*(3–4), 519–531, doi:10.1016/0012-821X(94)90088-4.

Viramonte, J. G., S. M. Kay, R. Becchico, M. Escayola, and I. Novitski (1999), Cretaceous rift related magmatism in central-western South America, *J. South Am. Earth Sci.*, *12*(2), 109–121, doi:10.1016/S0895-9811(99)00009-7.

Wegmann, M. I., U. Riller, F. D. Hongn, J. Glodny, and O. Oncken (2008), Age and kinematics of ductile deformation in the Cerro Durazno area, NW Argentina: Significance for orogenic processes operating at the western margin of Gondwana during Ordovician-Silurian times, *J. South Am. Earth Sci.*, *26*(1), 78–90, doi:10.1016/j.jsames.2007.12.004.

R. N. Alonso, Facultad de Ciencias Naturales, Universidad Nacional de Salta, 4400 Salta, Argentina.

B. Bookhagen, Geography Department, University of California, Santa Barbara, CA 93106, USA.

M. P. Hain, Department of Geosciences, Princeton University, Princeton, NJ 08544, USA. (mhain@princeton.edu)

H. Pingel and M. R. Strecker, DFG-Leibniz Center for Earth Surface Process and Climate Studies, Institut für Geowissenschaften, Universität Potsdam, D-14476 Potsdam, Germany.

A. K. Schmitt, Department of Earth and Space Sciences, University of California, Los Angeles, CA 90095, USA.